# Light Scattering by Atmospheric Particles – from Molecules to Birds

**Master's thesis**
**by**
**Patrik Lundin**

**Lund Reports on Atomic Physics, LRAP-413**
**Atomic Physics Division, Lund University**
**Lund, December 2009**

# Abstract

Lidar – acronym for *li*ght *d*etection *a*nd *r*anging – is a method where light is used to detect and investigate objects from a remote location. The most common medium under investigation is the atmosphere and small particles in the air itself, but also solid objects like vegetation and buildings can be examined. In this work, the light scattering by particles with sizes ranging from a few Ångström to more than a decimeter are examined as the lidar technique is used to study the elastic and inelastic scattering by molecules, by aerosol particles in the atmosphere and by, the comparatively huge, birds.

The versatile mobile lidar system in Lund, operated by the Atomic Physics Division, Lund University, has been developed and used for many years to measure pollutant gases, conditions of plants and historical buildings and much more. Until recently, it had not been used to investigate the vertical structure of the atmosphere, which otherwise is an important implementation of lidar systems. Neither had it been used in studies concerning living creatures. To take part in the first vertically sounding lidar campaign to map out the structure of aerosol particles, and to analyze the obtained results were two of the main purposes of this master's project. As the aerosol particles in our atmosphere are very much involved in the physics related to, e.g., global warming and the destruction of the ozone layer, this type of research is important and relevant to discussions today.

The other ambition of the thesis work was to get the lidar system implemented in the field of biology with a very novel approach to "probe" birds. The execution and the results of a field measurement campaign within this ecology-related area will be discussed.

The changing of the vertical structure of aerosol particles was revealed for a time period of four days. Promising results for the possibility of remote distinguishing between different bird species in flight were also obtained.

# Populärvetenskaplig sammanfattning

Detta examensarbete handlar om hur man kan använda optiska metoder för att på långt avstånd undersöka vår omgivning med inriktning på miljövetenskap.

LIDAR är namnet på en teknik som till principen är mycket lik radar. Med en radar sänds korta pulser av radiovågor ut och när de träffar ett föremål reflekteras delar av dem och registreras i en detektor positionerad på samma plats som sändaren. Genom att mäta tiden det tar från det att pulsen sänds ut till dess att den återkommer, kan man tillsammans med vetskapen om dess hastighet räkna ut avståndet till platsen där den reflekterades. Principen bakom LIDAR är densamma. Skillnaden är att man, istället för radiovågor, använder optiskt ljus som är antingen ultraviolett, synligt eller infrarött, och oftast sänds ut från en laser.

Tack vare ljusets egenskaper kan man göra så mycket mer än att bara mäta avstånd till stora föremål. Den fundamentala skillnaden mellan optiskt ljus och radiovågor är deras våglängder. Synligt ljus har en våglängd mellan 0,4 och 0,7 μm medan radiovågor ofta är flera meter långa. Då det krävs ett objekt som är minst lika stort som våglängden för att uppnå en effektiv reflektion, kan man alltså upptäcka, och mäta avstånd till, betydligt mindre föremål med LIDAR än med radar. Detta utnyttjas i allra högsta grad i första delen av arbetet presenterat i denna rapport, där ljusspridningen från enskilda molekyler och aerosolpartiklar i atmosfären studeras. Målet här är att med hjälp av det bakåtspridda ljuset från atmosfären ta reda på i vilka områden det finns mest aerosoler och hur detta ändras med tiden. I april 2009 användes därför det mobila LIDAR-systemet, uppbyggt vid avdelningen för atomfysik på Lunds universitet, på orten Vavihill i norra Skåne för att bland annat mäta fördelningen av aerosolpartiklar i atmosfären under fyra dagar. Även andra experiment utfördes under projektets gång och bland annat så studerades hur förändringen av laserljusets polarisation kan ge ytterligare information om atmosfären.

Då aerosolpartiklar i allra högsta grad är inblandade i olika fysikaliska och kemiska processer som bland annat påverkar klimatet på jorden och människors hälsa, är det oerhört viktigt att få en bra förståelse för hur dessa partiklar egentligen uppför sig och deras faktiska påverkan. Faktum är att den begränsade kunskapen inom området utgör en stor osäkerhet i de modeller som finns för att förstå jordens klimatförändringar. Att utveckla effektiva metoder för att mäta fördelningen av aerosoler i atmosfären är ett viktigt bidrag till att öka denna kunskap.

Med LIDAR kan man också mäta och kvantifiera andra egenskaper hos de föremål man studerar än bara *var* de befinner sig. Ett exempel på en variant av LIDAR-tekniken är att man studerar *fluorescensen* från det föremål man belyser med laserljuset. Fenomenet fluorescens uppstår då man belyser vissa material med ljus med en kort våglängd. Molekylerna i materialet blir exciterade och när de åter faller tillbaka till lägre tillstånd sänds bland annat ljus med längre våglängder ut. Exakt vilka våglängder detta är bestäms av de molekyler föremålet är uppbyggt av. Därmed, genom att studera färgen (våglängden) på det utsända ljuset kan man få en uppfattning om vad objektet man studerar är uppbyggt av och på detta vis identifiera okända ämnen och föremål.

Denna teknik används här för att studera, kanske något överraskande, fåglar. Olika fördelar med LIDAR kombineras för att på avstånd inte bara kunna se att och var en flygande fågel befinner sig men också av vilken art den är. Med hjälp av den höga känsligheten tekniken har, kan detta förhoppningsvis också göras på ett mycket stort avstånd, och eftersom ljuskällan är lasern i sig så utförs arbetet minst lika bra nattetid då en vanlig kikare inte fungerar.

Eftersom fåglar, med sin mobila livsstil, snabbt anpassar sig till klimatförändringar genom att flytta sina boplatser kan studier på dem indikera hur klimatet omkring oss förändras.

Varje år flyger miljontals fåglar mellan sina temporära boplatser i exempelvis Afrika och Europa. Detta bidrar starkt till det globala genflödet i allmänhet men också till spridning av sjukdomar. Som läget är just nu vet man inte exakt vart olika stammar av fåglar flyger. För att lättare kunna förebygga olika sjukdomar, till exempel de stora utbrott av fågelinfluensa som skett på senare år, så är det viktigt att flyttfåglarnas flygmönster bättre kartläggs.

# Contents

# Introduction

## I.1. Background

Ever since the industrial revolution in the end of the 18th and beginning of the 19th century, man's impact on Earth has grown rapidly to enormous levels. A very important factor is of course the steadily increasing global population, for the moment being 6.8 billion individuals, which all need food and shelter, things that, however, are not readily at hand in many parts of the world. Increasing needs for transportation and living standard have made human energy consumption and pollution impact a significant issue for the health of our planet.

Recently, the knowledge about how important it is that we try to minimize these impacts to create a sustainable environment has increased. Still, the situation is critical and tremendous global efforts have to be put into information, politics and research. Widely discussed today is the global warming – by many assumed to be created or increased due to human activities. This increase in temperature is certainly connected to the composition of the atmosphere surrounding Earth. And in fact, the knowledge about how the atmosphere is affecting the temperature and other climate related issues is something which needs to be improved to better understand how to meet these matters [1].

Birds, which adapt to the environment climate by, e.g., migrating between summer and winter seasons, might provide additional information of how the world is changing. The migration patterns of birds are also crucial to better understand the global gene flow and to know the function of the spread of bird carried diseases.

The lidar technique, using light to remotely investigate objects has proven to be one important tool to monitor, e.g., the changes in the atmosphere regarding a number of properties. With its large flexibility, the hope is that the technique could also be used to remotely observe birds and other creatures in flight.

The mobile lidar system operated by the Atomic Physics Division at Lund University has successfully been used to perform numerous different measurements over the years. It has acted at many locations, being used for measurements ranging from the mapping of dangerous exhaust gases from factories to work within the field of the preservation of cultural heritage. The methods used have among others been laser induced fluorescence (LIF), laser induced breakdown spectroscopy (LIBS) and most commonly differential absorption lidar (DIAL).

## I.2. Purpose of the work

As stated above, lidar is an important and globally widely used tool to quantify properties of the atmosphere surrounding Earth. However, the versatile Lund Lidar System had so far not been used to quantitively measure the total backscattering from the atmosphere.

Lidar systems have very recently been introduced in the field of biology (e.g. [2]) proposing a novel remote approach for animal monitoring. Neither this kind of research had yet been performed in Lund.

The general purpose of this thesis work was to take part in early trials to introduce the Lund Lidar System to the field of atmospheric aerosol investigations and animal monitoring. The aim was to explore the technical possibilities of the system and in the meanwhile gain information about the atmosphere. Regarding the studies on birds, this thesis work only includes early explorations about the potential for further work, and no specific results of biological value are presented.

## I.3. Methods

In cooperation with the Aerosol Group of the Department of Nuclear Physics at Lund University, lidar measurements were performed to map out the structure of aerosol particles in the atmosphere. The work was performed at the rural location Vavihill in northern Scania during four days in April, 2009. At the site at Vavihill, a background station is positioned to measure the air quality at ground level, and point monitoring data from the station were used in the subsequent analysis.

At a site by the river *Klingavälsån,* close to Veberöd, also in Scania, LIF was used with the purpose to discriminate between different species and genders of birds from a distance. Live Starlings and museum samples of other species were investigated. This project is a joint effort with the Migration Ecology Group of the Department of Ecology at Lund University.

The studies on birds were performed in connection with experiments regarding damselflies (Sw. ljungfrusländor) together with the Animal Ecology Group, also from the Department of Ecology. This is the reason for the chosen site by the river which is a preferred location for these insects.

## I.4. Layout of the report

The two different projects introduced will be discussed in Chaps 1 and 2, respectively. The layout of each chapter is to first introduce the relevant subject, then a section clarifying essential theory will follow, the equipment and setup are then described, the methods and results are presented as well as a discussion regarding the results obtained. After the two project chapters, there is a general discussion about future possibilities in the Outlook section, and a few details will be more thoroughly explained in the Appendix. As a final point the acknowledgements and references are presented.

As the study on birds will be presented in detail in an upcoming paper [3], this will not be discussed in detail to the same extent as the study on mapping the aerosol structure of the atmosphere.

## I.5. Summarized results

Lidar data were recorded during four days of field work at Vavihill. The data were analyzed and the altitude dependence of the scattering coefficient was determined for the same time period. Also, polarization effects were studied and it was found that the state of polarization

was distinctively more changed in the scattering event within clouds than in the surrounding air mass. Important information about the lidar system itself was also obtained.

Promising results were found for the possibility of remote bird classification with the help of laser induced fluorescence lidar. It was already in this first trial achievable to distinguish between a few museum samples of birds, and with refinements of the technique, the hope is that more species will be separable from a distance of up to 1 km.

# Chapter 1 – Vertical Sounding of Aerosol Particles

Aerosol particles are always present in the atmosphere and can be of both anthropogenic and natural origin. Aerosols are of great importance for the physics and chemistry of the atmosphere and thereby the climate. Human health is also affected by the composition of particles in the air, perhaps especially by the aerosols created by human activities [4]. It is very important that we get a more complete picture on how the aerosol particles are distributed in the atmosphere to better understand how they are affecting the global climate and health [1].

At a location named Vavihill, in northern Scania, Sweden, a background station is placed to measure aerosols and other properties of the air. This aerosol station is there to continuously, year around, evaluate airborne particulates and the concentration of a number of pollutant gases. The station is operated by, among others, scientists from the Aerosol Group of the Nuclear Physics Division at Lund University. The present experiments were performed in coordination with the Aerosol Group, which provided ground level data for comparison.

Lidar measurements were performed during four days in the spring of 2009, from April 6 to April 9. Participants in the measurements were, apart from the author, Ph. D student Zuguang Guan and Prof. Sune Svanberg, both from the Atomic Physics Division.

The background station at Vavihill for measuring, among other things, aerosol particles has a large number of devices to determine various properties of the air in Scania. A limitation in this type of measurements is that all these samples are taken at ground level. Of course, the composition at ground level gives some indication about the composition higher up in the atmosphere but it would be a great advantage to also directly measure the distribution of aerosol particles at different heights. This was also the main purpose of the lidar campaign; to determine the aerosol particle distribution in the atmosphere.

During the campaign, a number of features were studied. The aerosol particle distribution with altitude, the height of the clouds and polarization properties are of interest. Actually, multiple scattering and scattering by ice crystals and non-spherical particles in general will change the polarization state of light, but single scattering by spherical particles will not.

Regarding the measurement system, it is important to determine the apparatus function which is telling us how a totally homogenous atmosphere will be depicted and how possible saturation in the detector and other electronic effects will affect the measurements.

In view of further upcoming measurements, part of the purpose of the campaign was also to make sure that the system could readily operate without any external electricity supply. Therefore, during the four days in field, a 36 kW Diesel motor generator was used to supply all electricity needed. Such operation makes the system deployment independent of location.

A continuation of the work started with the measurements in Vavihill is to make similar recordings at other locations. In this way, the difference in air quality can be discovered and

out from such observations much important information can be extracted. The first comparative measurements are already being made and will continue to be performed in the major city Hangzhou in east China. Early data from the start-up of this campaign is included in the end of this chapter.

# 1.1. Theory

## 1.1.1 Earth's atmosphere

The gases that are kept as a layer around Earth by the gravitational force constitute the atmosphere. The gases are forming the air around us and the most abundant molecules are nitrogen to 78 percent, oxygen to 21 percent and argon to around 1 percent. Additional to these major constituents there is carbon dioxide, water vapor and a large number of other gases which are abundant only to trace amounts.

The atmosphere extends to around 100 km altitude, but since the air gets thinner and thinner further up in the sky, the limit between atmosphere and free space is indistinct. The atmosphere is divided into different layers with diverse properties. The lowest part, up to around 7 km at the poles and 20 km at the equator, is called the *troposphere*. This part of the atmosphere is where most of the weather occurs, and is also where the absolute majority of the aerosol particles are located. The lowest part of the troposphere is referred to as the *planetary boundary layer*, which is the layer where the air mass is noticeably affected by the friction from Earth.

Above the troposphere, the *stratosphere* is located, and the boundary between these two layers is called the *tropopause*. In the tropopause, a temperature inversion occurs, meaning that the temperature goes from decreasing with height in the troposphere, to increasing with height in the stratosphere. The stratosphere contains the *ozone layer*, situated at an altitude of around 20 to 60 km with a low concentration.

At even higher altitudes, the atmosphere stretches into the *mesosphere* from around 50 to 80 km and over this, the *thermosphere*, *ionosphere* and *exosphere* are situated, partly overlapping each other. However, these areas are reaching altitudes up to around 10.000 km and might not be considered to be part of the atmosphere.

The atmospheric gases are crucial for life on our planet in many ways; it provides conditions that both vegetation and animals need to survive. One important aspect is that the atmosphere protects us from part of the dangerous UV radiation from our sun. The oxygen in the air strongly absorbs all light with wavelengths below 200 nm and the ozone layer normally effectively protects us from the rest of the UV radiation below 300 nm [5].

Another important effect that the atmosphere has is the today widely discussed *green house effect*. The basic principle behind this is that the light from our sun, peaking in the visible region, to a relatively large extent can pass through the atmosphere and reach Earth. When Earth absorbs this light it gets warmer and starts to send out more heat, or infrared radiation. The atmosphere is not as transparent for this kind of radiation and a large fraction of it is

therefore absorbed or reflected back towards Earth, which therefore receives more energy than it would without the atmosphere. In this way there is a net increase of the temperature on Earth. This effect is very important for life, at least for humans. Without it the average temperature would be much less, making life here very difficult. What is extensively discussed today is the issue of the *extended* green house effect, which might be a consequence of human activities. Mainly hazardous in this aspect is the emission of carbon dioxide which is a strong green house gas.

### 1.1.2. Aerosol particles

An aerosol particle is an aggregate of matter that should be larger than single atoms or molecules but sufficiently small to be suspended in a gas. Generally when talking about aerosols one refers to small particles in the atmosphere. These can for example be small water droplets, pollen, smoke, etc. Dependent of the size of the particles, they can be divided into different classes. Particles with a diameter exceeding 2 μm are called *coarse*, while smaller particles, called *fine*, further can be divided into a *nucleation mode* and an *accumulation mode* with a size smaller or larger than 0.1 μm, respectively.

The aerosol particles play an important role for the climate of our planet. They are affecting the albedo[1] of Earth both directly and indirectly. The net effect is, as will be elucidated, complicated and depends on the size and type of particle, but generally aerosols are considered to decrease the temperature on Earth (e.g. [6], [7]). However, critical voices to this belief exist (e.g. [8]).

The most obvious direct effect that aerosols have on Earth's energy budget is how they can reflect incoming sunlight back into space, and how they can absorb and reflect the infrared radiation from Earth. These two direct effects can in some way work against each other since the first tends to decrease the temperature on Earth while the other tends to increase it.

The indirect effects are many since the aerosols influence several of the chemical and physical processes in the atmosphere. The knowledge about these indirect effects that aerosols have is still insufficient and considered to be one of the largest uncertainties in today's global climate models on "radiative forcing" [1]. One very important aspect is that the aerosols are vital for the advent and growth of clouds in the lower part of the atmosphere – the troposphere. The water droplets, constituting the clouds, are formed on and around a nucleus, which is generally an aerosol particle. The prevalence of these particles is therefore vastly affecting the speed and location of the cloud growth. Aerosols also affect the composition of droplet sizes, the effectiveness of the coalescence[2] and the freezing processes inside clouds. These effects

[1] An object's albedo is the extent to which it diffusely reflects light from the Sun. An albedo of 0 means that no light is reflected and 1 means that all light is reflected.

[2] Coalescence is, in this context, when the smaller water droplets in the clouds merge together to form larger drops.

lead to a change in both the albedo and the precipitation. The latter is also very important since it determines the lifetime of clouds.

Another example of an effect that the aerosols have is the destruction of the ozone layer. For the same reason as above, the amount of aerosol particles is crucial for the creation of stratospheric clouds at the poles. These clouds consist of small ice crystals with a large surface-to-volume ratio, making them ideal as a location for chemical reactions to occur. In some of these reactions, free, reactive chlorine is formed, which is working as a catalyst for ozone destructing reactions. One of the most well known reactions is that of chlorine with ozone forming hypochlorite and oxygen molecules. The hypochlorite can then react with the oxygen radical to form chlorine and oxygen molecules, after which the first reaction can start all over (see Eq. 1.1-1).

$$\begin{aligned} \mathrm{Cl} + \mathrm{O_3} &\rightarrow \mathrm{ClO} + \mathrm{O_2} \\ \mathrm{ClO} + \mathrm{O} &\rightarrow \mathrm{Cl} + \mathrm{O_2} \end{aligned} \tag{1.1-1}$$

As mentioned, aerosols can be of both natural and anthropogenic character. The latter ones are mostly due to wood burning and combustion of coal and oil [9]. In unclean combustion processes, large amounts of sulfate aerosols are created, now being at such a level that anthropogenic sulfate is dominant over the natural ones in the atmosphere [9]. Combustion also creates soot, which is a widespread aerosol that in fact leads to a net increase of Earth's temperature [10], [11]. As is well known, different kinds of combustion also constitute one of the main causes for the increase of the eminent green house gas carbon dioxide in the atmosphere. It is therefore without doubt crucial that the issue of developing clean and efficient replacements for combustion is taken acutely, both in research and politics.

Examples of aerosols that are not created by human activities are volcanic particles and desert dust. Both these types are highly influencing the climate. Desert dust, e.g., from Sahara, consists of mineral grains which both reflect and absorb sunlight. The absorption is causing an increased temperature in the parts of the atmosphere where the particles are. This increased temperature is in turn considered to suppress rainfall over desert areas [9].

It is easy to realize that the consequences aerosols have on the climate of Earth are enormous. It is therefore also very important to get a more thorough understanding of their exact effects, and to evaluate the role humans play.

### 1.1.3. Important concepts regarding light

History has revealed that in order to fully tell the nature of light, two different explanations are needed. This experience is generally referred to as the *duality of light*. One part of the explanation is that light is a wave, propagating in the energy transport direction, and the other part is that light consists of small weightless quantized particles – *photons*.

The wave explanation states that light is electromagnetic radiation consisting of a coupled electric and magnetic field, oscillating from side to side, creating a wave of energy. The

colour of the light is determined by the frequency of these oscillations. Together with the speed of light in the medium in which it travels, the frequency also determines the wavelength. The relationship between these properties is given by Eq. 1.1-2.

$$\lambda = \frac{c}{\nu}, \tag{1.1-2}$$

where $\lambda$ is the wavelength, $c$ is the speed of light and $\nu$ is the frequency.

In the particle explanation, each of the photons is seen as a bundle of quantized energy and it is in this quantization that the major difference between the explanations is hidden.

A wave of light is said to have a certain *polarization*. The polarization is a measure of the direction of the oscillations. By convention, the polarization is said to be the direction of the oscillations of the electric part of the wave. Depending on how the direction of the electric and magnetic field vectors change as the wave travels, the light is referred to as either linearly, circularly or elliptically polarized – the latter being the general case.

A laser, which is the light source in the lidar system, generally generates linearly polarized light, where the directions of the field vectors and oscillations are constant with propagation.

## 1.1.4. Scattering

One of the most important physical phenomena within the lidar field is *scattering*. Scattering can occur when a photon interacts with an object in its way.

### 1.1.4.1. Elastic scattering

As the electrons and protons that constitute the atoms and molecules are electrically charged, complex electronic and magnetic fields are created within. This fact does not only help to make it possible for the atoms and molecules to stick together, but these charges also provides the possibility for interaction with light, which as stated, as well can be described as electronic and magnetic fields.

Most likely, the atom or molecule is found in its ground state, which has the lowest of the discrete possible energies of the particle. But when interaction with the surrounding occurs, the atom or molecule can temporarily transfer into another energy state. This interaction may for example be that it scatters light. A scattering event on a particle like this can be described as that the photon influences the particle to quickly shift from one energy state to another, higher lying, and then back again[3]. When the particle returns to its original state, it again sends out a photon. This can happen in any direction and there are thorough theories describing the probability for emission in different directions depending on the circumstances.

[3] The higher-lying energy state can also be a so called virtual state. Because the scattering process is so quick, the atom does not have to shift to a real state but it can also use this extremely broad virtual state.

If, as described here, the final state in this scattering process has the same energy as the original one, the scattering is referred to as *elastic scattering*.

The most commonly described elastic scattering processes are Rayleigh scattering, which is the dominant when the object is smaller than the wavelength of the light, and Mie scattering, which is more dominant when the object is larger than the wavelength.

The photon may also be absorbed and the atom transferred to a real excited state so that the light is reemitted after an in comparison long time period. The phenomenon is then better referred to as resonant radiation than as elastic scattering.

#### 1.1.4.2. Raman Scattering

If the energy of the final state, on the other hand, is different from that of the original, the scattering process is instead said to be inelastic. This is generally entitled *Raman scattering*. Since the energy-shift for the atom when it *absorbs* one photon, is then different from that when it *emits* the other, the energy of these two photons will also differ from each other. Because the energy of these two photons is different, the wavelength must also have changed.

Also *fluorescence* is based on the same physics, but also here the time scale is longer than for the case of scattering. As this phenomenon forms the basis of Chap. 2, it will be more discussed there.

If the energy of the emitted photon is lower than that of the absorbed, the Raman process is further referred to as *Stokes scattering*, and in the contrary case the process is called a*nti-Stokes scattering*. Evidently, for the latter process to occur, the molecule or atom must from the beginning be found in a state different from the ground state. Since this under most conditions is unusual, the process of anti-Stokes scattering also becomes rare in comparison.

The positions of the energy levels are specific for every atom or molecule, and therefore the same applies to the energy- and wavelength shifts in the inelastic scattering processes. Thus, by observing the shift in wavelength, or colour of the light, the object it was scattered on can be identified.

### 1.1.5. Lidar

In contrast to some animals, such as bats, humans do not have any direct ranging capability. However, other systems, as for example radar, using radio waves, have been developed to give us the ability to solve this problem. Lidar – short for *li*ght *d*etection *a*nd *r*anging – is the counterpart utilizing optical radiation.

The lidar technique was first developed in the 1930's using flashlamps [12], but with the help of the introduction of the laser in the 1960's and its rapid development during the 70's, 80's and 90's, the technique was improved a lot to become an important research tool and also an industrially available product.

The essential components of a lidar setup are a light source, transmitter optics, receiver optics, a detector and some kind of analyzing equipment. In Fig. 1.1-1, the principle of lidar is shown with the help of two of the key components – a laser and a detector.

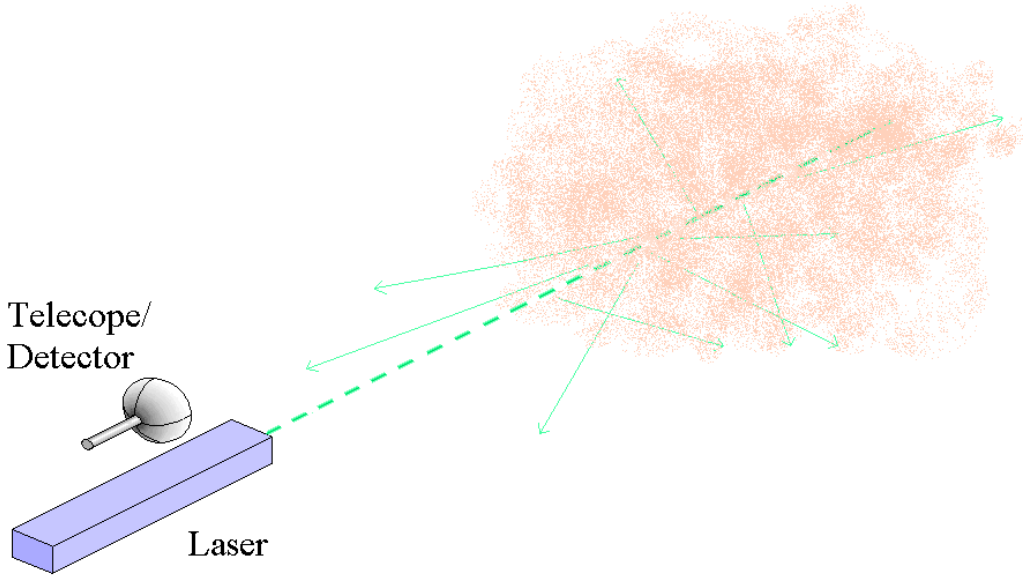


Fig. 1.1-1. The principle of lidar. A laser beam consisting of short pulses is sent out into some kind of scattering medium, represented by the cloud. The particles or molecules scatter the light in all directions and some of the photons are scattered backwards, towards the detector. The time between the transmitted pulse and the arriving photons at the detector is measured, and by knowing the speed of light, the distance to the scattering object is obtained.

The basic principle is that either a short light pulse or a modulated wave of light is sent out from a laser. If photons are reflected on an object, and are arriving at the receiving optics and the detector, the echo signal can be used to measure the distance to the object in question. If a pulsed light source is used, the time between the transmitted pulse and the received photon is measured, and by dividing this time with the speed of light multiplied with two (back and fourth), the distance is obtained. The distance, $d$, in a lidar measurement is therefore given by Eq. 1.1-3.

$$d = \frac{\Delta t \cdot c}{2}, \tag{1.1-3}$$

where $\Delta t$ is the elapsed time and $c$ is the speed of light in the medium of interest. To have a good range resolution it is important to have sufficiently short pulse duration since this, together with the detection speed, ultimately sets the resolution. In Fig. 1.1-2, a schematic diagram of the most important parts of the transmitting and receiving optics in the lidar setup used in this work are presented.

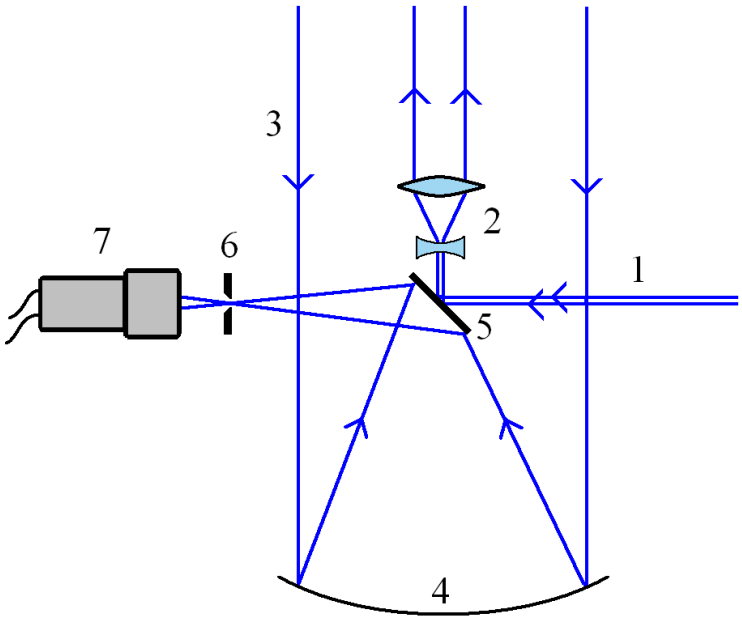


Fig. 1.1-2. The transmitting and receiving optics in the lidar setup used. Components included in the figure are: 1) beam from the laser, 2) expanding optics, 3) returning scattered light, 4) focusing telescope, 5) folding mirror, 6) aperture and 7) detector.

An important advantage that lidar has in comparison to radar is the short wavelength of light compared to the longer wavelength of the radio waves. Since objects with a size at least in the same order of magnitude as the wavelength are required to appreciably scatter or reflect light, lidar can study much smaller objects.

Lidar can thus be used both to study small particles, and large objects like vegetation and buildings. When studying these larger objects, it might generally not be the distance that is the most important goal of the measurements, unless we deal with a military range finder. Instead, different variations of the technique, as for example, laser induced fluorescence lidar, are used to study other properties of the object. Since this technique is used in the work presented in Chap. 2, it will be described there. The scattering on very small objects is although what is important for the work presented in this chapter.

When studying the atmosphere, a laser pulse (or a modulated signal), is sent out into the air. The scattering is not occurring at a single location but minute fractions of the light is scattered throughout the whole path of the laser beam. A small part of the photons will be scattered backwards with a chance to arrive the detector. The amount of photons scattered in a certain area gives an indication about the properties of the air just there. In this way a *lidar curve* is shaped, containing information about the atmosphere, and hopefully also about the aerosol particles within.

The general lidar equation is given by Eq. 1.1-4.

$$P(R) = K\beta(R)\mathrm{e}^{-2\int_0^R \alpha(r)dr} / R^2 \quad (1.1\text{-}4)$$

Here, $P$ is the signal at the detector, $K$ is a system constant, $\beta$ is the backscattering coefficient representing the amount of light scattered directly[4] backwards per unit distance, $\alpha$ is the extinction coefficient representing the fraction of light that is lost per unit distance and $R$ is the distance. Both $\beta$ and $\alpha$ contain parts arising from both molecular scattering and particle scattering. Therefore $\beta$ can be written as $\beta = \beta_p + \beta_m$ and $\alpha$ as $\alpha = \alpha_p + \alpha_m$. Further, the aerosol and molecular part of the extinction can both be divided into absorption and scattering with a resulting extinction coefficient given by $\alpha = \alpha_p + \alpha_m = \alpha_{p,A} + \alpha_{m,A} + \alpha_{p,S} + \alpha_{m,S}$ (subscript $m$ represents molecule, $p$ particle, $A$ absorption and $S$ scattering). In some areas where the air is unclean, the molecular part of the extinction and backscattering coefficients are considered to be negligible compared to the particle part, leading to $\beta = \beta_p$ and $\alpha = \alpha_p$. These assumptions are used (e.g. [13]) but have to be done so with caution. That the absorption part of the scattering is low for our conditions is confirmed through ground level measurements done *in situ* (see Appendix). One assumption that is not very dangerous to make though, is that the molecular part of the extinction and scattering can be considered to be varying modestly with height compared to the particle part.

The molecular part of the extinction in clean air at ground level pressure for light with 355 nm wavelength is around 0.075 km$^{-1}$ [14]. This part of the extinction is then assumed to fall off with altitude with the same dependence as that describing how the air density decreases with height. The density falls off proportionally to the decrease in pressure with height, which approximately follows an exponential relation, as in Eq. 1.1-5 [15].

$$p = p_0 e^{-z/H_e}, \quad (1.1\text{-}5)$$

where $p_0$ is the pressure at ground level, $z$ is the altitude and $H_e$ = 7321 m is the height where the pressure has dropped to 1/$e$ times the value at ground level [15]. This equation can be re-written as Eq. 1.1-6.

$$p = p_0 2^{-z/H_2}, \quad (1.1\text{-}6)$$

where $H_2$ = ln(2)·7321 m = 5088 m is the height at which the pressure is half its value at sea level[5].

[4] ”Directly” backward is here referring to an angle sufficiently close to 180 degrees to reach the detecting system.

[5] The height at which the pressure is decreased to half the sea-level-value depends on the specific conditions and therefore the value differs between references. Commonly it is though stated to be between 5.0 and 5.6 km.

In the theoretical Eq. 1.1-4 above, $K$ is as mentioned a system constant. This constant is representing the efficiency of the transmitting and receiving optics, the power of the laser system, the efficiency of the detector, etc. The specific value will not play any part in the later analysis but another thing is very important; $K$ cannot at all be considered to be independent of range in the practical case.

The main reason for this is the *geometrical compression* of the lidar signal at close range [16]. The principle of this compression of the lidar signal is presented in Fig. 1.1-3. Here, the telescope has been represented by a lens instead of a mirror for better understanding. The function is basically the same but it is easier to follow the light pathways.

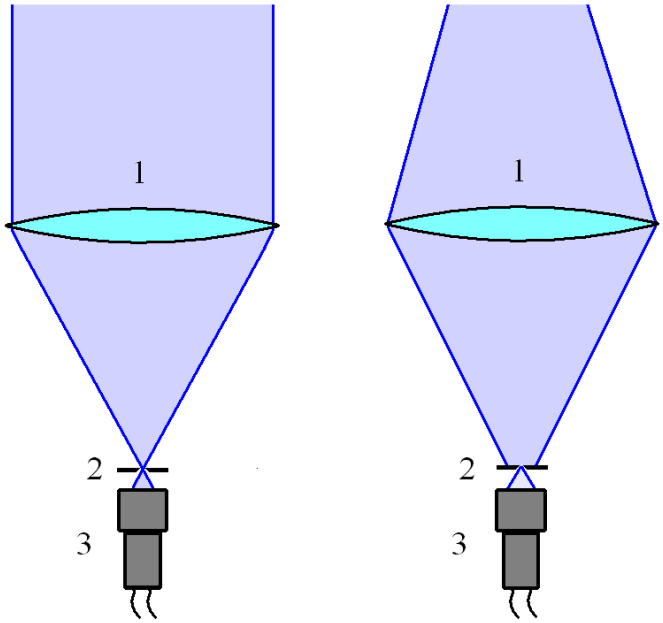


Fig. 1.1-3. Schematic illustration of the principle of geometrical compression. In the figure the telescope is represented by a lens (1). Also included are the aperture (2) and the detector (3). The left figure represents scattering from long distance and the right figure represents light scattered at close distance.

The figure to the left is showing light from the far field and the figure to the right is representing light scattered at short distance. When the light from the far field returns, it can be considered to be of parallel nature. A circular aperture is placed in the focal plane of the telescope, and the parallel light is focused here. Because of this, all light can pass through the aperture in this case. The light scattered at close distance (approximately below a couple of hundred meters in most cases) on the other hand, is not parallel. This light is therefore focused further back, behind the aperture. Due to this, a fraction of this light is lost, and the effect gets more significant the closer the scattering event is taking place. This effect, referred to as geometrical compression, is therefore discriminating the near field scattering, giving rise to a modification of the general lidar curve which otherwise is similar to a $1/R^2$ polynomial. The effect is schematically shown in Fig. 1.1-4.

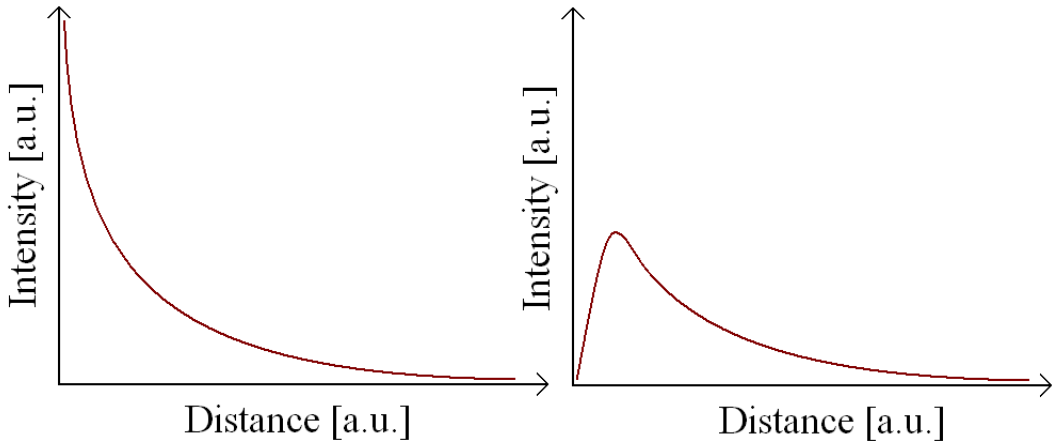


Fig. 1.1-4. The effect of geometrical compression. To the left, a curve without any geometrical compression is shown, and to the right this effect is taken into account.

With the assumption of only particle scattering, no absorption and the range dependent system constant one ends up with a modified lidar equation given by Eq. 1.1-7.

$$P(R) = K(R) \cdot \beta_p(R) \, \mathrm{e}^{-2\int_0^R \alpha_{p,S}(r)dr} / R^2 \tag{1.1-7}$$

## 1.1.6. Obtaining the aerosol particle distribution

The recorded lidar curves are simply the intensity of light at the detector (or rather the number of photons arriving the detector per time interval) as a function of time. This is the raw data but it is generally not what is shown when one sees a lidar measurement of the aerosol distribution or the humidity in the air. What is more commonly presented is instead the scattering coefficient, $\alpha(R)$. Since the scattering coefficient is highly connected to the concentration of particles in the air, it is a good indication of the aerosol distribution in the atmosphere.

### 1.1.6.1. The Klett inversion method – one-component case

A powerful *lidar inversion method* – a method to receive the scattering or extinction coefficient from a lidar curve – was presented already in 1969 [17]. This inversion method can be used in the case when a simple relationship between the backscattering coefficient and the extinction coefficient can be assumed. This relationship is that $\beta = \alpha^k/S$ , where $k$ is a constant between 0.7 and 1.3 and $S$ is a constant representing the inverse of the fraction of the scattered light that can be considered to be scattered backwards. The related inversion equation is shown in Eq. 1.1-8.

$$\alpha(R) = \frac{X(R)}{X(R_f)/\alpha(R_f) - (2/k)\int_{R_f}^{R} X(r)dr} \tag{1.1-8}$$

Here $X(R)$ is the lidar signal compensated for the $1/R^2$ dependence and the varying system constant. Thus $X(R) = P(R)\cdot R^2/K(R)$. $R_f$ is a chosen reference distance at close range. The value of the scattering coefficient has to be known or estimated at the reference distance.

Another requirement for this method to be completely satisfactory is that the scattering from aerosol particles should be much stronger than the one from molecules [13]. This is generally only the case with measurements done at urban areas or positions where the air is unclean for other reasons. In our measurements which are performed at a location far from factories and urban areas, the assumption of non-clean air would not be very true.

The inversion method from 1969 has been shown to be quite unstable and sensitive to mis-estimates of the scattering coefficient at the reference distance [18]. Therefore James D. Klett presented a new inversion method in 1981, where the reference value was set at a far distance instead. This method leads to Eq. 1.1-9:

$$\alpha(R) = \frac{X(R)}{X(R_f)/\alpha(R_f) + (2/k)\int_R^{R_f} X(r)dr} \tag{1.1-9}$$

To be able to use this method, first $X(R)$, being the lidar signal compensated for all (geometrical fall-off and range depending system properties) but the dependence of extinction, has to be obtained. The principal way in theory, when the system constant is considered to be just that – a constant – is simply to multiply $P(R)$ with $R^2$. In the practical case, $K$ is as discussed not a constant but is rather also depending on $R$. To also consider this, other approaches have to be used. One way is to employ some sort of reference curve for the short range where these effects are important, which should simulate how a totally homogenous air mass is described by the system. This is, however, a difficult task. To know if the sky is homogenous, the scattering has to be measured. But to measure the scattering one has to have a calibrated system. One method frequently used is simply to obtain a reference curve during a day which "seems" clear, when you can assume that there are little or no structures in the air. However, in this work another approach was used.

### 1.1.6.2. The Fernald inversion method – two-component case

Since also the Klett inversion method is only valid for situations when the aerosol scattering can be considered to be much stronger than the molecular one, i.e. when the air is not very clean, it is not satisfactory for our purposes and therefore an improved theory has to be applied. This theory is the *Fernald inversion method*, or the two-component case method, presented in 1984. The basic idea of this is similar to the Klett method but now the scattering from air molecules is also considered. The lidar equation (still under the assumption of negligible absorption) is, with molecular scattering included, written as Eq. 1.1-10.

$$P(R) = K(R)\cdot(\beta_p(R)+\beta_m(R))\,\mathrm{e}^{-2\int_0^R(\alpha_p(r)+\alpha_m(r))dr}/R^2 \tag{1.1-10}$$

As before, a simple relation between the backscattering and the total scattering is assumed, namely that $\beta_m = \alpha_m/S_m$ and $\beta_p = \alpha_p/S_p$. Also here, $S$ can be approximated as a constant both for the molecular and the particle part [19]. For the molecular part, Rayleigh theory can be employed, leading to $S_m = 8\pi/3$ (e.g. [19], [20]), but for the particle part the situation is more complex. The backscattering ratio is highly dependent on the size and refractive index of particles and the value can therefore vary a lot. Generally, the restriction is that $S$ should be between 0 and 90 [21], even though a value below one is very unphysical since this limit corresponds to that *all* scattered light is scattered backwards. The reason that 0 is still sometimes used for $S_p$ is that this provides a solution where no corrections are made for attenuation from aerosol particles.

The inversion will now, with the molecular scattering considered, be based on Eq. 1.1-11 presented by Frederick G. Fernald.

$$\alpha_p(R) = -\frac{S_p}{S_m}\alpha_m(R) + \frac{S_p \cdot X(R)\exp\left\{2\int_R^{R_f}\left[\frac{S_p}{S_m}-1\right]\alpha_m(r)\mathrm{d}r\right\}}{X(R_f)\Big/\left(\alpha_p(R_f)/S_p + \alpha_m(R_f)/S_m\right) + 2\int_R^{R_f} S_p \cdot X(r)\exp\left\{2\int_r^{r_f}\left[\frac{S_p}{S_m}-1\right]\alpha_m(r')\mathrm{d}r'\right\}\mathrm{d}r} \qquad (1.1\text{-}11)$$

### 1.1.6.3. The Raman reference method

There is in the atmosphere to the largest extent nitrogen, which as previously stated is abundant to around 78 percent [22]. The aerosol particle concentration is negligibly small compared to the one of nitrogen, so even if there are clear structures in the concentration of aerosols and other particles and clouds, the concentration of nitrogen will stay more or less the same. Of course, the concentration of nitrogen has a general drop with height since the air gets thinner. As shown before, the atmospheric pressure is approximately half the sea level value at 5100 meters and the same is true for the concentration of nitrogen.

As the concentration of nitrogen is independent of the aerosol structure, a lidar curve where only the scattering from nitrogen is considered would be a very effective way to obtain a reference curve representing a homogenous mass.

To be able to only observe the scattering caused by nitrogen molecules, the nitrogen Raman shifted lidar signal is recorded. This has frequently been done (e.g. [23], [24]).

The lidar equation for a recording obtained in the Raman shifted mode is given by Eq. 1.1-12.

$$P_R(R) = K \cdot \beta_R(R)\,\mathrm{e}^{-\int_0^R (\alpha_{\lambda_0}(r)+\alpha_{\lambda_R}(r))dr}/R^2, \qquad (1.1\text{-}12)$$

where $\beta_R(R)$ is the Raman backscattering coefficient, $\alpha_{\lambda_0}$ is the scattering coefficient (or actually the extinction coefficient, but absorption is still ignored) at the laser wavelength and $\alpha_{\lambda_R}$ is the scattering coefficient at the Raman shifted wavelength. If a curve obtained in the elastic mode is divided with a curve obtained in the Raman shifted mode, Eq. 1.1-13 is obtained.

$$\frac{P_0(R)}{P_R(R)} = \frac{\beta_0(R)}{\beta_R(R)} \cdot \frac{e^{-2\int_0^R \alpha_{\lambda_0}(r)dr}}{e^{-\int_0^R (\alpha_{\lambda_0}(r)+\alpha_{\lambda_R}(r))dr}} = \frac{\beta_0(R)}{\beta_R(R)} \cdot e^{-\int_0^R (\alpha_{\lambda_0}(r)-\alpha_{\lambda_R}(r))dr}, \quad (1.1\text{-}13)$$

where $\beta_0(R)$ is the backscattering coefficient at the laser wavelength.

For a simplified solution to the problem it can be assumed that the total scattering is more or less the same at the laser wavelength as at the Raman shifted wavelength. In this way, the exponent in the expression after the second equal sign in Eq. 1.1-13, approaches zero, and the exponential factor comes close to one. The backscattering coefficient at the laser wavelength can then be written as in Eq. 1.1-14.

$$\beta_0(R) \approx \frac{P_0(R)}{P_R(R)} \cdot \beta_R(R) \quad (1.1\text{-}14)$$

Since the backscattering coefficient at the Raman shifted wavelength, $\beta_R(R)$, can be assumed to follow a strict exponential height decreasing pattern with a value that is dimidiated at approximately 5100 meters, all right hand side expressions in this equation are now known and the result can readily be obtained.

To improve the results, the effect of the non-zero exponential factor in Eq. 1.1-13 can also be considered, leading to Eq. 1.1-15.

$$\beta_0(R) = \frac{P_0(R)}{P_R(R)} \cdot \beta_R(R) \cdot e^{+\int_0^R (\alpha_{\lambda_0}(r)-\alpha_{\lambda_R}(r))dr} \quad (1.1\text{-}15)$$

The equation has to be solved in an iterative way. First, as given by Mie and Rayleigh theory, a wavelength dependent relationship is assumed between the total scattering at the laser and Raman wavelength (see Eq. 1.1-16).

$$\frac{\alpha_{\lambda_0}}{\alpha_{\lambda_R}} = C_1\left(\frac{\lambda_0}{\lambda_R}\right)^{-2} + C_2\left(\frac{\lambda_0}{\lambda_R}\right)^{-4}, \quad (1.1\text{-}16)$$

where $C_1$ and $C_2$ are coefficients determined by the amount of scattering by particles and molecules, respectively[6].

With the by Eq. 1.1-6 obtained values for $\alpha_{\lambda_0}(R)$, the backscattering coefficient at the laser wavelength, $\beta_0(R)$, is calculated a first time according to Eq. 1.1-15. As a following step, $\alpha_{\lambda_0}(R)$ is re-calculated as $\beta_0(R)\cdot S_p$ where after $\beta_0(R)$ can be better approximated. This process is iterated until the backscattering coefficient remains unchanged through two subsequent iteration steps.

## 1.2. Equipment

The Lund Lidar System, presented in Fig. 1.2-1, is built up inside a Volvo F610 truck. The vehicle contains equipment composed to create a versatile mobile lidar system with transmitting optics, receiving optics, electronics, cooling systems and air-conditioning systems.

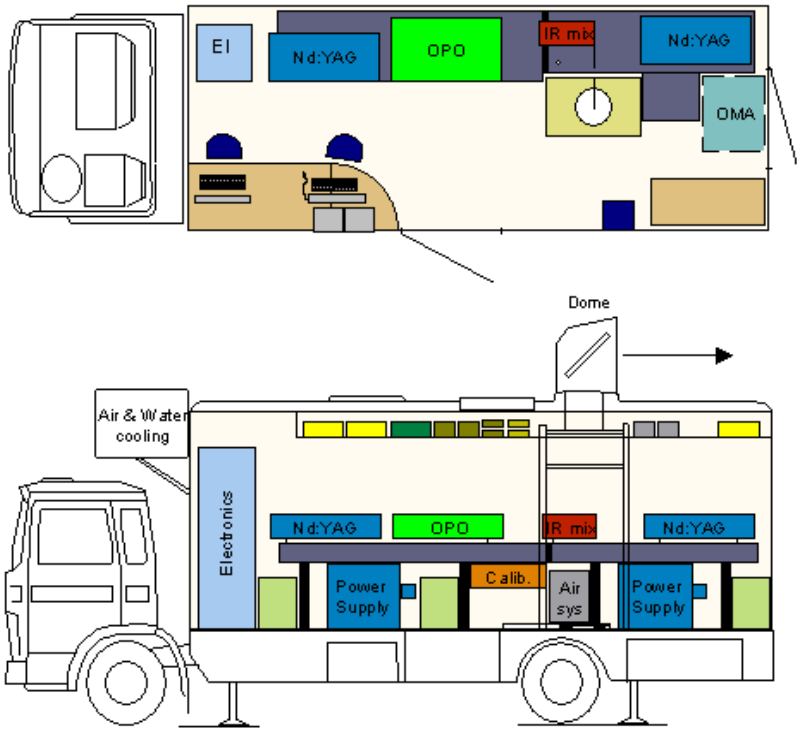


Fig. 1.2-1. The setup of the lidar system used in the work presented in this thesis (modified from [25]).

The basic setup of the system is that one of two lasers produces short pulses at 355, 532 or 1064 nm, which can be used either directly, or shifted in wavelength with the help of an

[6] The exact values on $C_1$ and $C_2$ are not easily accessible but do anyway only set the initial guess for $\alpha_{\lambda_0}(R)$. Misestimates will sort themselves out in the iteration process.

*optical parametric oscillator* or an *IR-mixer*[7]. The laser pulse is then sent out from the dome on top of the roof via a beam expander (see Fig. 1.1-2), enabling the divergence of the beam to be chosen to fit the task and to ensure a safe performance. Inside the dome, a rotatable mirror is placed to allow the beam to be scanned in the vertical direction. Also, the dome itself can be turned around the vertical axis to enable the beam to be steered in any direction, 360 degrees around the truck. In front of this tunable mirror, a quartz window, transparent for all wavelengths used, is placed, protecting the inside equipment from rain, etc.

The returning light, coming from the outside, is reflected on the same mirror down onto a 40 cm in diameter Newtonian telescope, situated directly under the dome (see Fig.1.1-2). The telescope is focusing the collected light onto a fast detector – a *photomultiplier tube,* or *PMT*[8] – which records the signal as a function of time. The detector is triggered by the emission of a pulse from the laser to set the time zero, from which the distance information is later obtained. The signal is then sent to computers for analysis. Most of the system is controlled from the computers and the handling is based on the software LabVIEW®. To allow use in rural areas, a 36 kW Diesel motor generator is used to supply the electricity needed for the equipment.

The lasers used are Nd:YAG lasers from *Spectra Physics*, producing light pulses of around 3-5 ns duration at 20 Hz repetition rate. During the experiments in Vavihill, the pulse energies were chosen depending on the specific purpose, but in general they were in the order of 25 mJ.

A more thorough description and specifications of the system can be found in [25].


Fig. 1.2-2. The lidar truck used at field campaign during spring, 2009.

[7] Since the optical parametric oscillator and IR-mixer are not used during the measurements, the function of these will not be discussed further.

[8] As detectors, photomultiplier tubes (PMT's) are used throughout this work. The principle of this kind of detector is described in the Appendix, section A2.

# 1.3. Obtaining a reference recording

During the analysis of data from the Vavihill site, two different methods have been explored to retrieve the scattering coefficient: The *Fernald inversion method* and the *Raman method*, both discussed in the theory section.

As the system constant, $K$, is dependent on the range, at least for the short range signal, it is as stated not enough to multiply $P$ with $R^2$ to obtain $X$ which is used in the inversion. Instead the approach of using a reference curve, supposed to be recorded in a homogenous air mass was employed.

The inhomogeneity of the particle distribution in the atmosphere is frequently assumed to be mostly in the vertical direction (e.g. [26], [27], [28]). The atmosphere can supposedly be divided into several layers, each with its own properties. This feature of the atmosphere is useful to attain a calibration when measuring the vertical distribution of aerosols. One could by obtaining a lidar curve in the horizontal direction, assuming horizontal homogeneity, have a reference for the apparatus function of the system. Therefore, data was recorded with the system in the mode of horizontal send out, averaging over about an hour. Horizontal homogeneity is of course an approximation since the sky clearly does not look the same everywhere and there are also critical voices raised to this approach as well (e.g. [29]).

There are, however, a number of problems or obstacles with the implementation of this method that have to be overcome before any accurate results can be obtained. The most important of these issues are presented with the corresponding solutions below.

## 1.3.1. Loss of exponential behavior

When using a reference curve instead of a simple $1/R^2$ fall of to obtain $X(R)$, all the behavior except for the structures in the atmosphere is lost, including some of the fall-off arising from the exponential factor in Eq. 1.1-11. The reason is that even if the scattering coefficient is assumed to be constant with distance in the reference recording, it is for sure not zero. That part (or all) of the exponential factor is lost for $X(R)$ is not desired, since only the geometrical properties and the $1/R^2$ fall-off should be compensated for. Therefore, this (presumably constant) exponential factor, $\alpha$, has to be detached from the reference curve, $G(R)$ before use. But as can be seen in Eq. 1.1-11, in order to remove this factor, it has of course to be known. Thus, to be able to calculate the height dependence of $\alpha$ for the vertical curve, an estimate of $\alpha$ itself but now on ground level, has to be used to correct the reference signal.

The molecular extinction coefficient for clean air at ground level pressure for 355 nm light is as declared assumed to be 0.075 $km^{-1}$. The particle induced extinction coefficient at ground level is provided by data from the background station. A mean value of this part during the time of the recording of the reference curve is 0.030 $km^{-1}$. The total extinction coefficient is the sum of these two and is thus equal to 0.105 $km^{-1}$. This value can now be used to compensate for the exponential behavior of the reference curve.

### 1.3.2. Reference for longer range

The horizontal curve, which is used in the calculations, was obtained with a maximal range of 3500 meters while many of the signals that should be analyzed were recorded with a range up to 7.5 km. A reference for the distance after 3500 meters therefore had to be added. The reason for this difference in range is that in the vertical mode, both the dome and the quartz window were dismounted, enabling a more direct light path. The signals were thus, as reasonable, stronger in the vertical mode, so this height could be reached.

For this long range, the geometrical compression, etc., has without any doubt stopped to play any important role, and therefore it is quite straight forward to simply insert a $1/R^2$ fall off to the reference here.

### 1.3.3. With and without window

The horizontal reference curve is, as stated, recorded with the system in the mode that the dome together with its quarts window was mounted while most of the signals that should be analyzed were obtained without these components. The reference curve should therefore be compensated for any artifacts that this difference might create.

This is done in the way that during a time period, data were obtained where it was quickly alternated between having the window installed and not to find out what effect it actually had on the measurements. A mean value of several recordings with and without window is shown in Fig. 1.3-1.

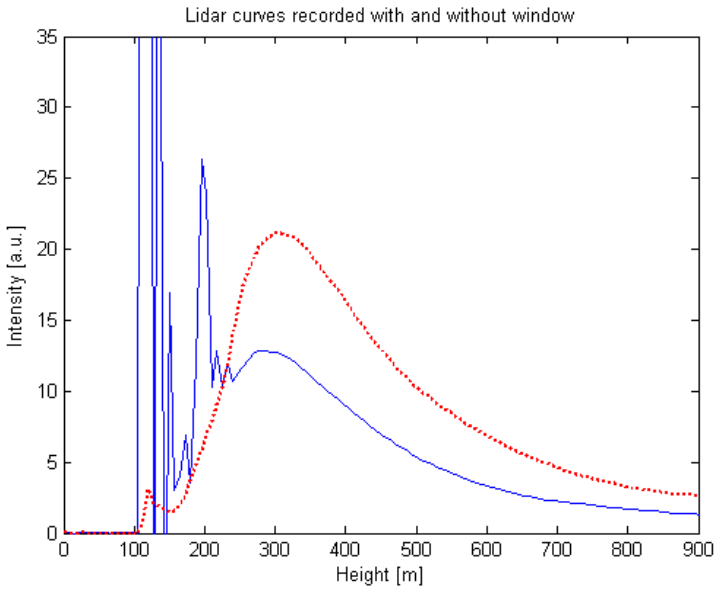


Fig. 1.3-1. Recording made with the quartz window shown in solid line (blue) and a recording made without the window shown in dotted line (red).

The most dominant effect that the window has, except for decreasing the entire signal, is that it creates a large reflex that resides in the electronics and affects the first part of the range. To compensate for this behavior, the horizontal curve which should be used as a reference is

(under the assumption of a linear signal influence) multiplied with the ratio between the signal without and with window.

# 1.4. Measurements and results

A number of different experiments were performed during the campaign. The means of the execution and the results of these will be presented in this section. The major part is the analysis of the particle distribution, which is basically composed by the calculation of the height dependence of the scattering coefficient, $\alpha$, described in the theory section. Other experiments discussed are a study of how the polarization of the transmitted laser light is changed in the scattering processes at different heights and a few trials where different properties of the equipment itself are studied.

From the background station in Vavihill, reference values of the particle scattering coefficients at ground level were provided with the help of a nephelometer. These scattering coefficients were measured at 700, 520 and 450 nm. Our laser was though positioned at 355 nm where no reference value was provided. Therefore, a second-degree polynomial extension was made to estimate the ground level coefficient at 355 nm from the values for the other three wavelengths (Mie scattering, which is considered to be dominant, is proportional to $\lambda^{-2}$). This ground reference value was used in the way that the calculated variation of the scattering coefficient was "locked" to the reference so that the scattering coefficient was forced to have the ground level reference value at low altitude. The approach of using data from a nephelometer as reference in lidar applications has been utilized before (e.g. [30]).

A large part of the purpose of the campaign at Vavihill was to obtain raw lidar data during an extended time period in order to monitor the change in the properties of the atmosphere. It was arranged for automatic recording and periodical read out of lidar- and background signals and storage with time and date information.

## 1.4.1. Aerosol particle distribution

### 1.4.1.1. The Fernald inversion method

When the three issues stated above were solved for the reference curve, the apparatus function for the system was known and $X(R)$ could readily be obtained from the raw recorded signals $P(R)$. The Fernald inversion method was then employed on the large amount of collected lidar data. The processing was done in the software Matlab®.

Profiles of the scattering (or rather extinction) coefficient were obtained for the atmosphere above Vavihill for the four days of the campaign. Examples of profiles for the scattering coefficient are shown in Figs 1.4-1, 1.4-2 and 1.4-3.

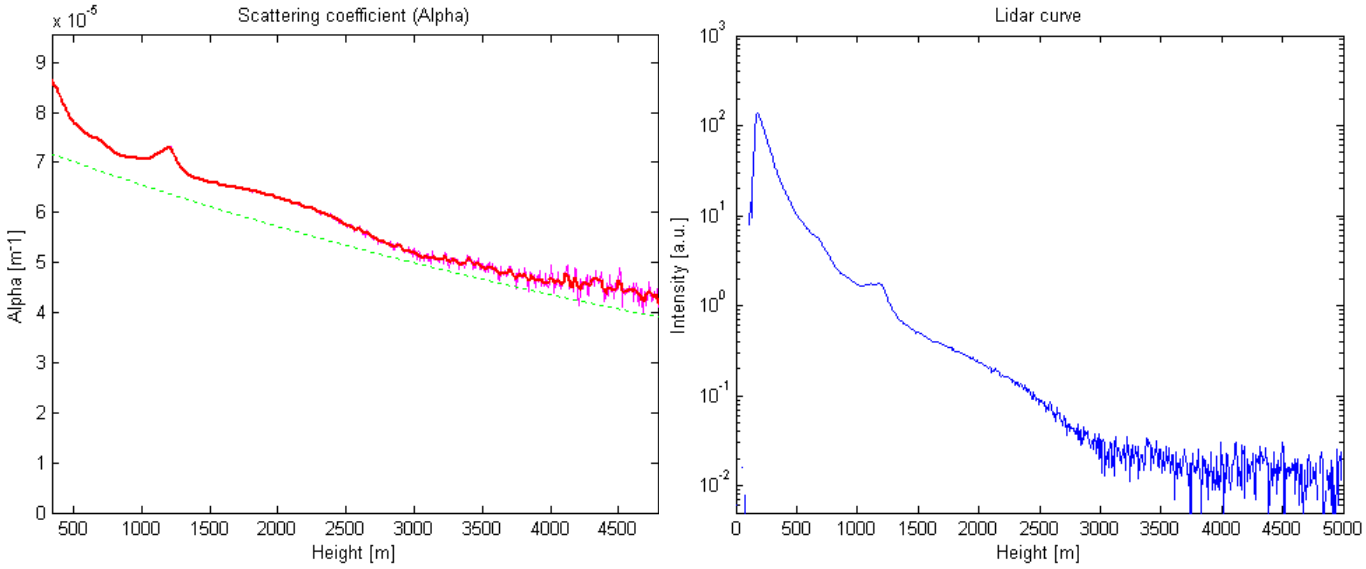


Fig. 1.4-1. To the left: Scattering coefficient profile calculated with the Fernald method. The dashed line in green represents the molecular scattering and the solid line in red is the sum of the molecular and the particle scattering. The measurement is done at 18:15 on April 7. To the right: The corresponding raw lidar curve in logarithmic intensity scale.

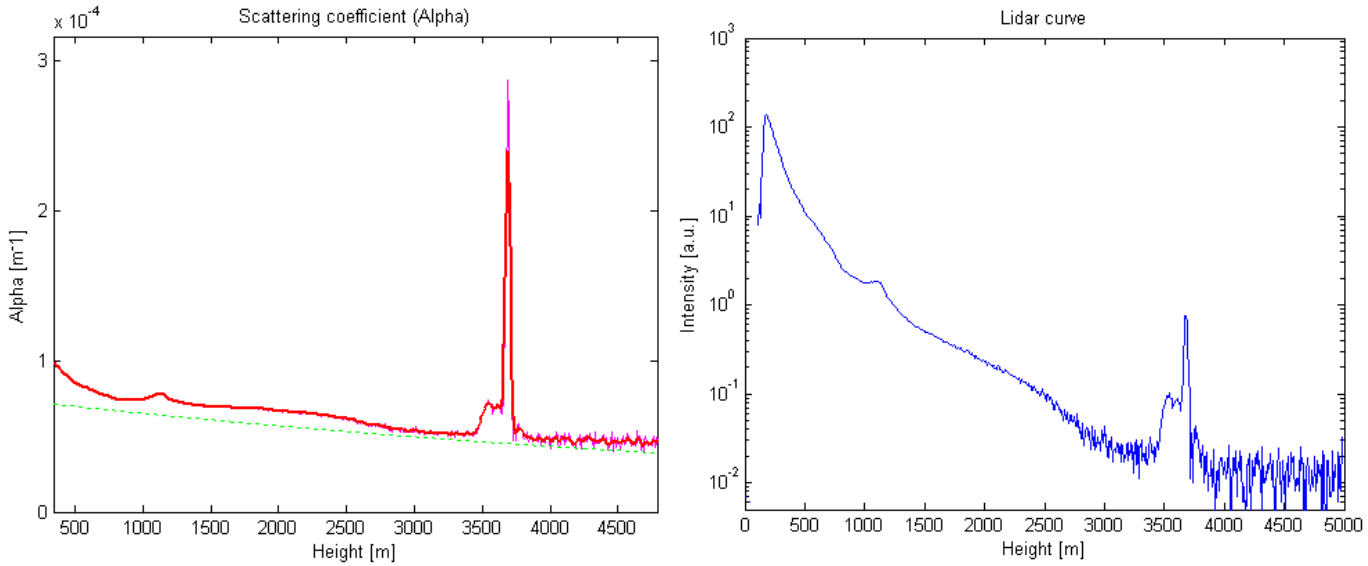


Fig. 1.4-2. To the left: Scattering coefficient profile calculated with the Fernald method. The dashed line in green represents the molecular scattering and the solid line in red is the sum of the molecular and the particle scattering. The measurement is done at 18:30 on April. A sharp cloud is seen at an altitude of around 3.6 km. To the right: The corresponding raw lidar curve in logarithmic intensity scale.

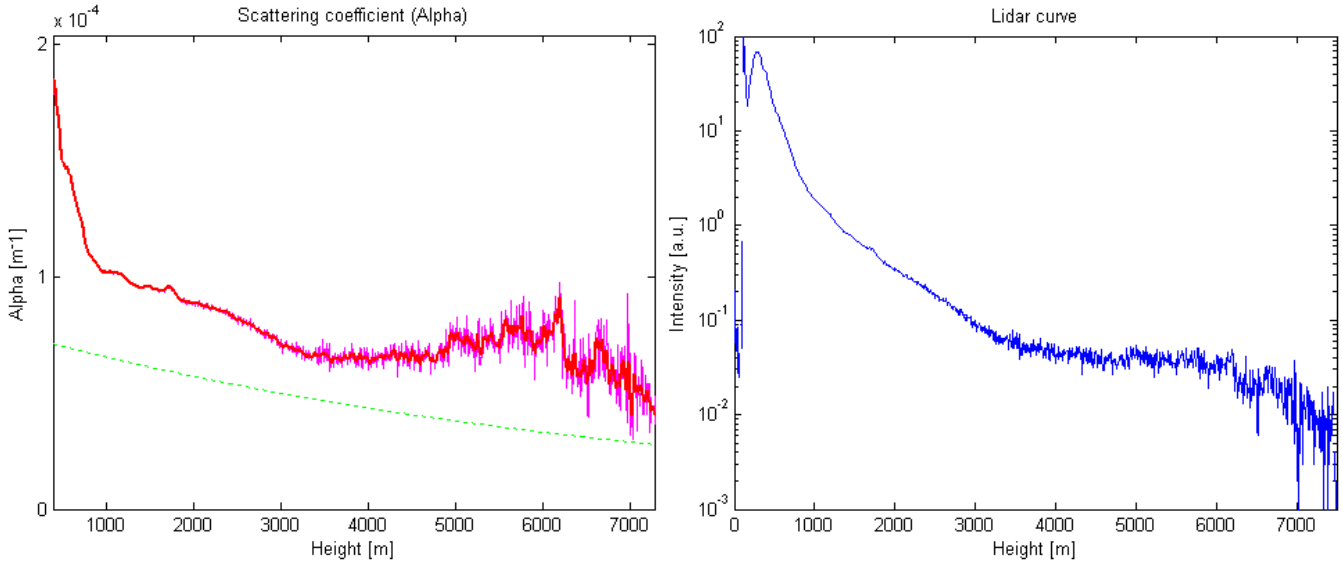


Fig. 1.4-3. To the left: Scattering coefficient calculated with the Fernald method. The dashed line in green represents the molecular scattering and the solid line in red is the sum of the molecular and the particle scattering. The measurement is done at 20:20 on April 8. An extended area of increased scattering is observed at altitudes around 4 – 7 km. To the right: The corresponding raw lidar curve in logarithmic intensity scale.

### 1.4.1.2. The Raman reference method

The Raman shift for nitrogen is 2331 $cm^{-1}$ [31] which with a laser at 355 nm results in a signal at 387 nm. Therefore an interference filter for 387 nm light was placed in front of the PMT and lidar curves were obtained. One example of the results is shown in Fig. 1.4-4 where the mean signal of two curves obtained with the 387 nm interference filter is shown in blue. In between the recordings of the Raman signals, elastic curves were also obtained, and the mean value of those is shown in red.

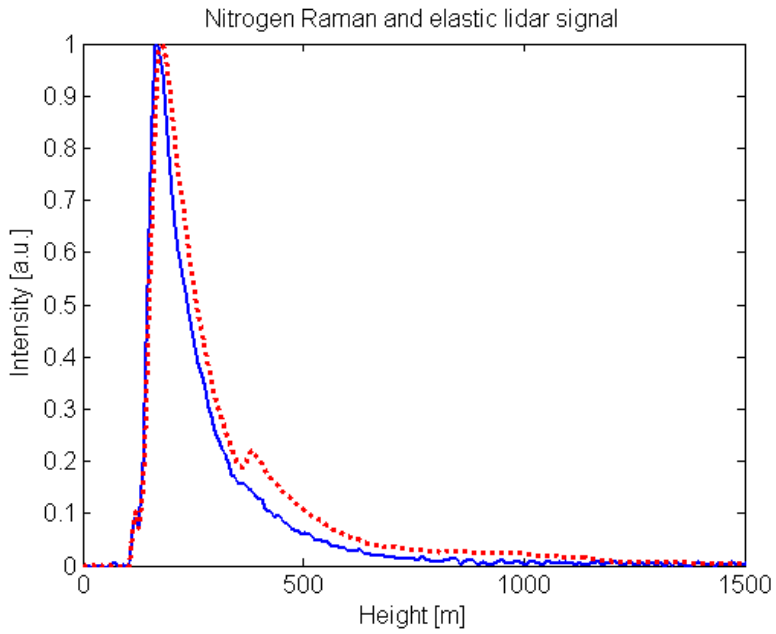


Fig. 1.4-4. The mean value of two lidar recordings of nitrogen Raman shifted signals in solid blue and the same for two elastic curves shown in dotted red. The curves are normalized with regards to peak-value to each other for easier comparison. If they would not, the elastic signal would be many times stronger than the Raman shifted one. It can be observed that the aerosol structure which is clear for the elastic signal is not as present in the Raman shifted one. Noticed can also be that the Raman signal is noisier in the tail which is a direct consequence of the weakness of the signal.

With this approach it can be made clear how a structure of the atmosphere that is visible in the elastic signal, is not as visible in the Raman signal. It seemed promising to use the nitrogen Raman signal as a reference to the other!

However, if the Raman signal is studied carefully at longer range, the noise can be seen. This comes as a direct consequence of the inherent weakness of the signal. As the mathematical processing of the signal is quite sensitive to this kind of noise, the outcome is everything but good. The scattering coefficient calculated with the help of Eqs 1.1-15 and 1.1-16 is thus very unstable.

With this signal quality of the Raman recording it was unfortunately thus concluded that this approach was impossible to use.

### 1.4.1.3. Final Results

One of the ambitions with the campaign was to gather data for an extended time period to be able to see how among other things the scattering coefficient changed during the days and during the week. Therefore the best functioning method – the Fernald inversion method, was employed to calculate the scattering coefficient for a large amount of data collected during the four days of the field campaign. The summarized result is presented in Figs 1.4-5 and 1.4-6. The first figure is showing the total scattering coefficient from both aerosol particles and molecules and in the second one the molecular part is subtracted to more clearly illustrate the structures from particles.

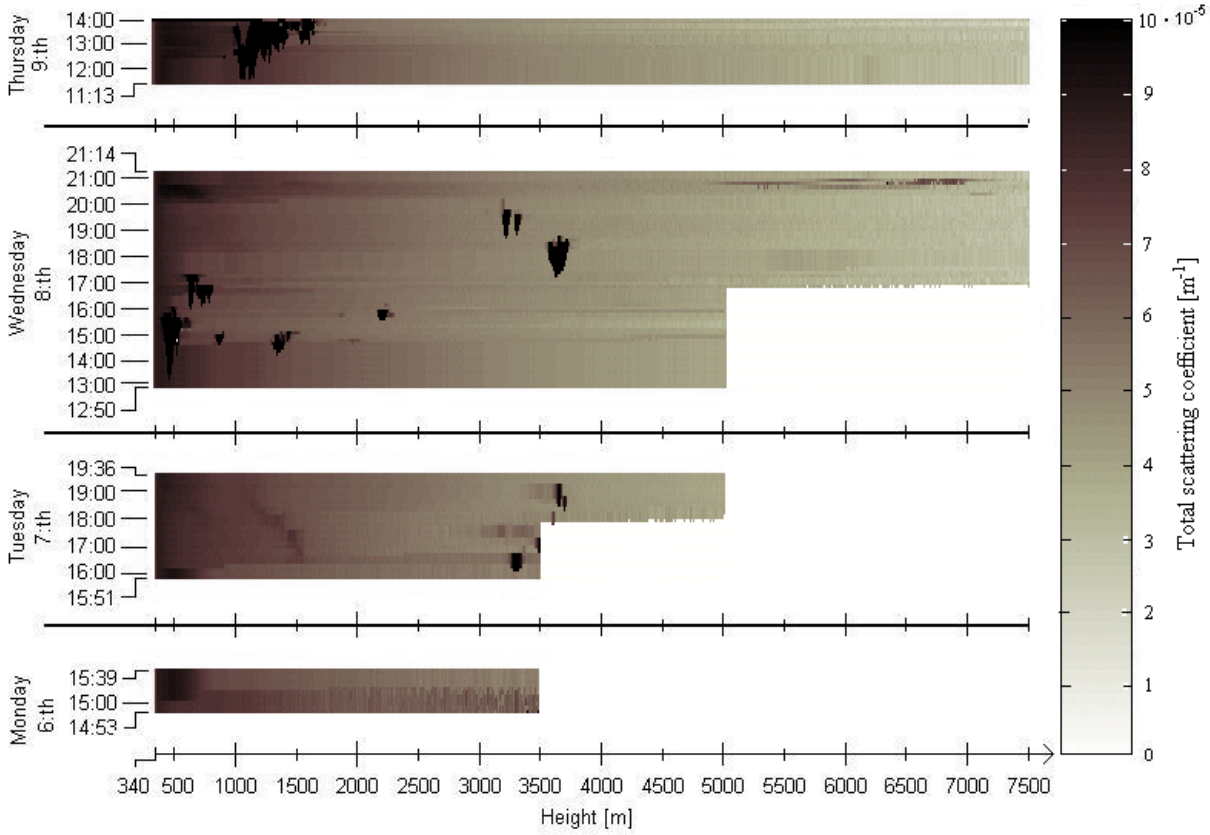


Fig. 1.4-5. The total scattering coefficient calculated for the measurements done during the time April 6-9, 2009, at Vavihill. The left (y) axis shows the times for the recorded data in hours and minutes.

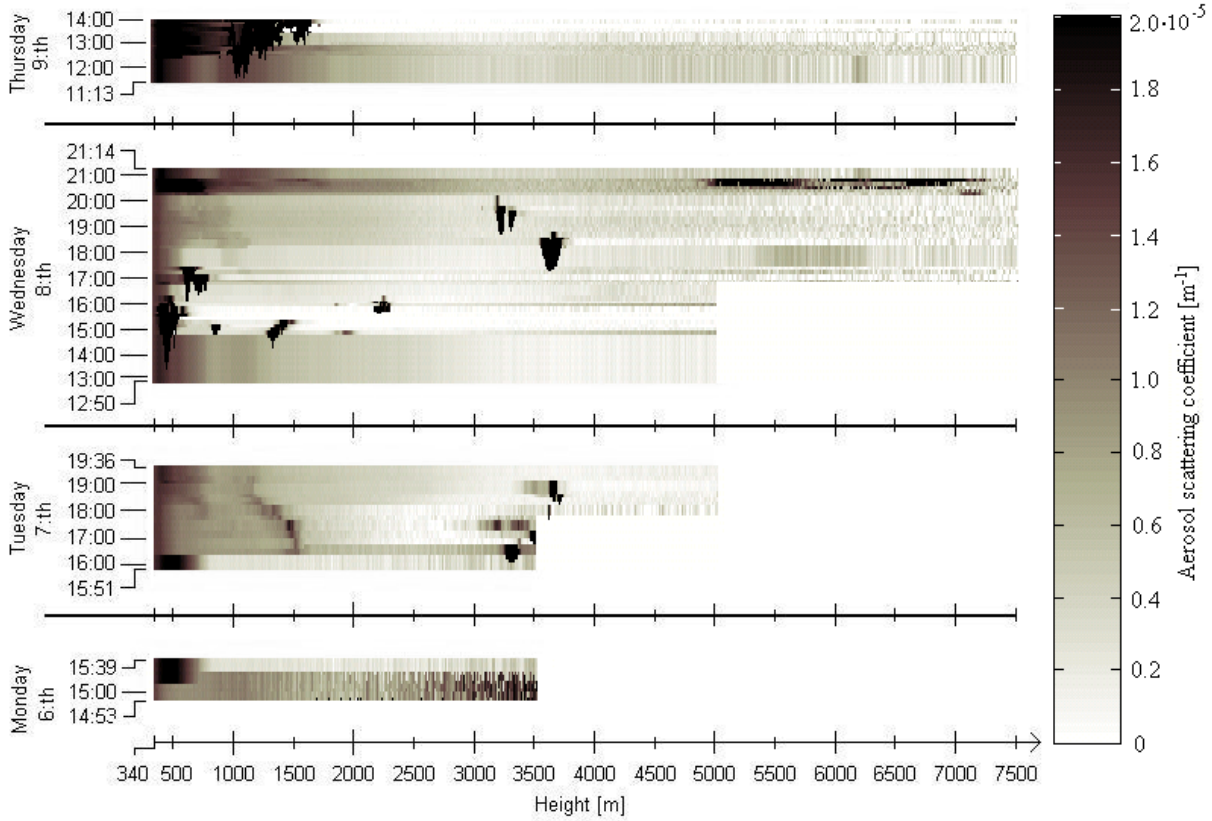


Fig. 1.4-6. The scattering coefficient only considering aerosols calculated for the measurements done during the time April 6-9, 2009, at Vavihill. The left (y) axis shows the times for the recorded data in hours and minutes.

The reason the range is shorter for the data for the 6th and the 7th is simply that light for longer ranges are not recorded during that period. Different improvements made it possible to increase the range in the later part of the Campaign.

Other experiments performed during the four days, which were more or less sophisticated, will be presented in the following sections. Some were meant to explore the atmosphere, others were purely meant to investigate the performance of the system.

In sections 1.4.2 to 1.4.5, some of these experiments are discussed. The first section (1.4.2) is dealing with how the polarization of the light is changed when scattered at different heights. The other three sections (1.4.3 – 1.4.5) are concerning how different settings are affecting the results. The latter three sections might not be very interesting to the general reader but are rather documentations for further work.

## 1.4.2. Depolarization

To study how the polarization of the light sent out by the laser into the atmosphere is changed in the scattering events is one way to investigate properties of the air and clouds. A simple model of scattering says that single scattering on a spherical particle will not change the polarization, but both multiple scattering and scattering on non-spherical particles will. Of course, very few of the aerosol particles are perfectly spherical, but a large fraction can nevertheless be considered as that. Water droplets in clouds are one example of almost perfectly spherical particles since this shape is the best way to minimize the surface energy. Because of this, single scattering in low clouds does generally not change the polarization of the laser light. High clouds, however, which are located where the temperature is low, are

often consisting of small ice crystals which are not spherical at all. Therefore the polarization is thought to change in these clouds, and this should be noticeable when studying the polarization status of the light arriving at the detector.

In this experiment, first of all the polarization status of the laser light was tested by positioning a polarization filter (a polarizing cube) in the laser beam after the internal optics. This showed that the light from the laser was as expected well polarized.

The routine of the implementation was that lidar curves were recorded with the polarization filter placed in front of the PMT inlet. Between every other series of recordings, the light-passing-direction of the filter was alternated between perpendicular and parallel with regard to the polarization of the transmitted light.

In general, the signal when having the filter in the perpendicular direction was very low compared to that in the parallel direction. This can be seen in Fig. 1.4-7 as the difference between the dash-dotted curve in green, which represents light with perpendicular polarization and the dashed curve in blue which is light with parallel polarization.

During the measurements, a cloud was located at around 1000 meters altitude. This cloud could be observed in both polarization directions but the relative signal strength from the cloud compared to the rest of the air was much greater in the case of perpendicular polarization. Actually, the height of the cloud slightly differs between the measurements with the two polarizations. However, this was compensated for by artificially placing the peak positions at the same altitude in the figure. The mentioned relative strength of the cloud in the two polarizations is seen clearly when the signal for perpendicular light is amplified so that the close range signal strength is matched for the two polarizations. This is shown as the solid curve (red) in Fig. 1.4-7 to the left. It can be noticed how the relative signal from the cloud scattering is much greater in the perpendicular light curve. This experiment shows that there is either multiple scattering or scattering by non-spherical particles in the cloud to a significantly greater extent than in the air below. By taking the ratio between the curve for light polarized perpendicular to the laser light, and the curve for light with parallel polarization, the same thing is even more obvious. This is presented in Fig. 1.4-7 to the right, where a distinct increase in the ratio is noticed at the height where the cloud is located.

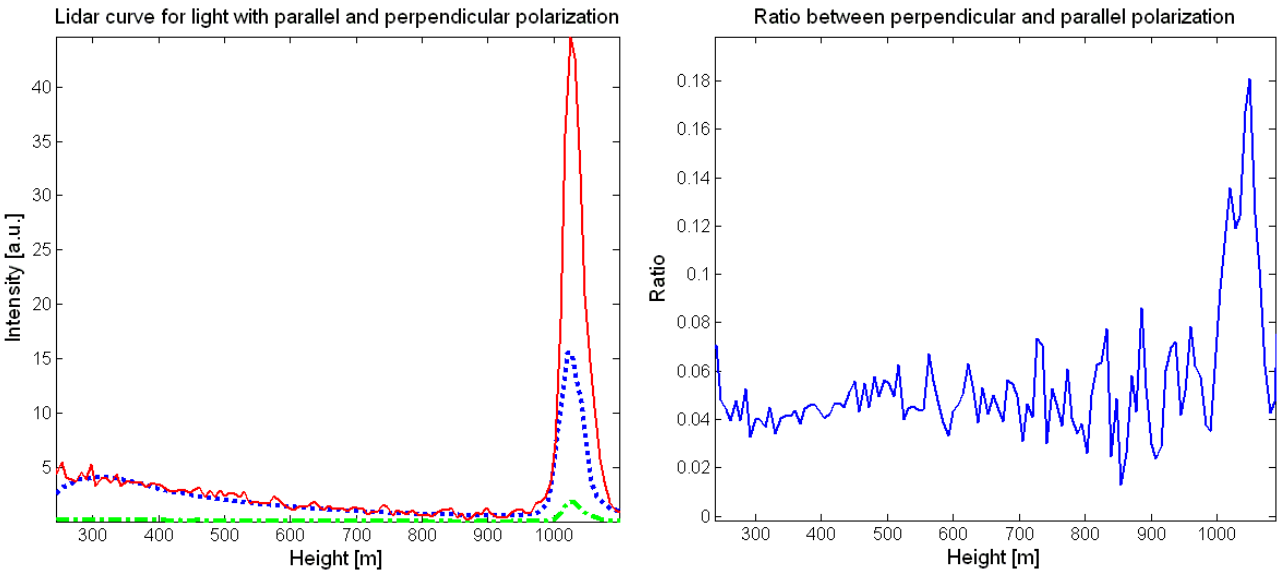


Fig. 1.4-7. To the left: the lidar curves for light with polarization parallel with and perpendicular to the transmitted laser light. The solid line (red) is light with polarization perpendicular to the transmitted laser light amplified to, at close range, match the signal for light with polarization parallel to the transmitted light shown in dashed line (blue). The dash-dotted line (green) is the signal for light with perpendicular polarization without amplification. To the right, the ratio between the signal for light with polarization perpendicular to, and parallel with the transmitted light is shown.

## 1.4.3. Impact of aperture size

As schematically shown in Fig. 1.1-2 in the theory section, there is an iris or aperture placed in the light pathway before the detector. By changing the size of this it is possible to change the geometrical compression conditions described in section 1.1.5. By having a small aperture in front of the detector, the light from the close range is discriminated as this light is more out of focus than that scattered further away. Geometrical compression is constantly present since the aperture size is always limited, but by decreasing the size of this, the effect becomes more prominent. It should also be mentioned that if a beam with small divergence is used, the effect of geometrical compression is more significant than if the beam has a large divergence. If a large beam divergence is used, the aperture always has to be larger than with a small divergence.

In this experiment, an additional aperture was placed 11.5 cm behind the focus (where the original aperture is). A collimating lens is positioned shortly after the original aperture making the light from the far field again parallel. The close field light is however not perfectly parallel but diverges slightly. At the position of the second aperture, once again the close field is thus affected more by this spatial limitation. At this position, the geometry is, on the other hand, “magnified” and the effect is more easily studied. However, it not self evident that an aperture at this position actually has the described effect. For a qualitative simulation of the optics background to these “loose” arguments see Appendix A.3.

The size of the second aperture was alternated between a diameter of 8 mm (referred to as "with aperture") and 20 mm (referred to as "without aperture"), which actually is the physical limitation of the inlet to the detector, and the effect of the signal was studied.

Several recordings were made with and without the aperture. One example is shown in Fig. 1.4-8 where the solid curve in red shows a case with the large opening and the dotted curve in blue shows a case with the small opening. In the figure it is obvious that the aperture is discriminating the signal from close range. To clearer show what is happening with the far field signal, the ratio between the two curves is presented in Fig. 1.4-8 to the right. This can be seen to increase at close range but to keep roughly constant for the far field, where the signal also gets noisier. By fitting two straight lines[9] to the ratio it can be shown how the aperture is affecting the signal. The small aperture is discriminating the close range and then the signal light is let through more and more up to a certain limit (at around 6-7 hundred meters in this case) after which the aperture is not affecting the signal anymore.

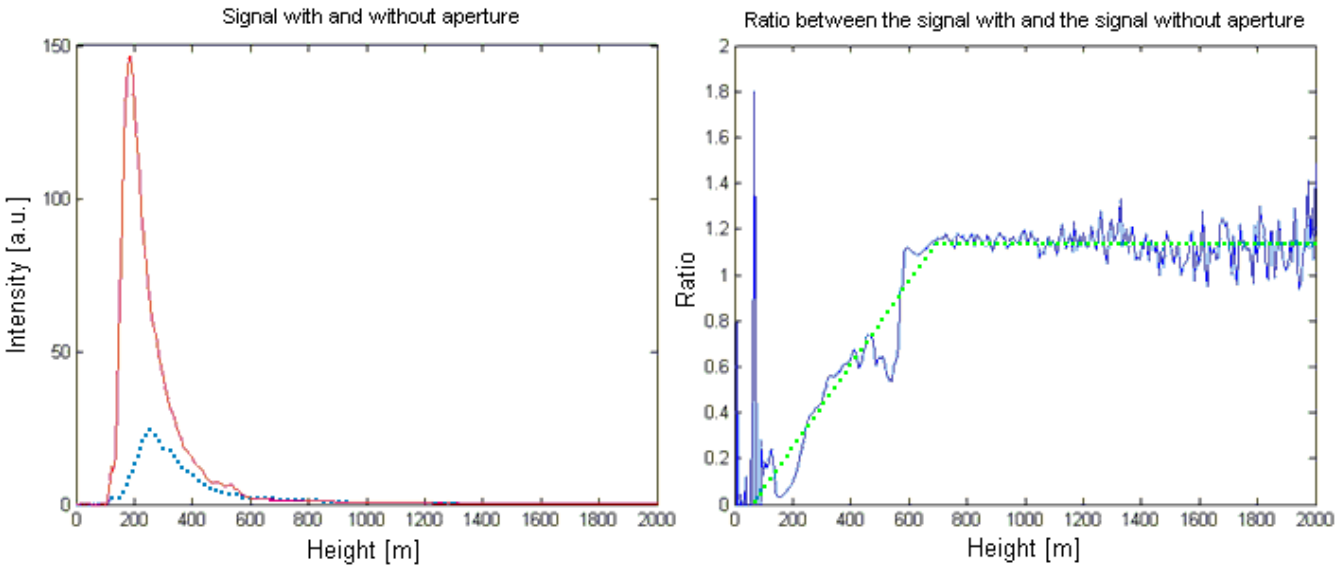


Fig. 1.4-8. To the left lidar signals recorded with (dotted, blue) and without (solid, red) aperture are shown. To the right the ratio between the two signals is shown in solid line (blue). Two straight (dotted) lines are fitted to the curve to simulate how the aperture is affecting the signal.

[9] That it should be straight lines, corresponding to first degree polynomials, and not polynomials of a higher degree is not self evident, but this suits both the simulation and experimental results. Depending on the exact geometry of the optics, this behavior could change.

### 1.4.4. Saturation in the PMT

One critical demand for getting reliable results is that no saturation in the detection occurs during any of the recordings. It is crucial that the output signal from the detector is a well defined function of the incoming amount of light. In this case the signal from the PMT should be proportional to the incoming number of photons per time interval.

There are mainly two causes for saturation in photomultipliers. One phenomenon can occur at the cathode[10]: if too many photons come in at the same time, they fill up the cathode completely and any more photons will therefore not contribute to the signal. This is not likely to happen in this lidar mode since the light arriving the detector is always quite weak. The other possible phenomenon could take place at the dynodes: when the current between two dynodes becomes large, it is hard to keep the voltage between them constant. If the voltage drops, this will in its turn reduce the current and the signal is automatically decreased.

To make certain that this is not the case in the measurements, an experiment employing a neutral density filter was performed. During a period of reasonably clear sky, a number of recordings were made where high signal strength was achieved for some distance. Further, recordings were also made under similar conditions with a neutral density filter placed in front of the detector. The function of the density filter is to lineally reduce the intensity of the light arriving at the detector. In this way, a curve should appear with the exact same shape as without filter, but with the signal decreased by a certain factor at all points. If the detector, on the other hand is working poorly, the *shape* will also be changed. If saturation is present, this means that the detector discriminates points with high intensity and gives out a too low value for these. Then, when the filter is inserted the signal strength will be reduced *less* where saturation occurs.

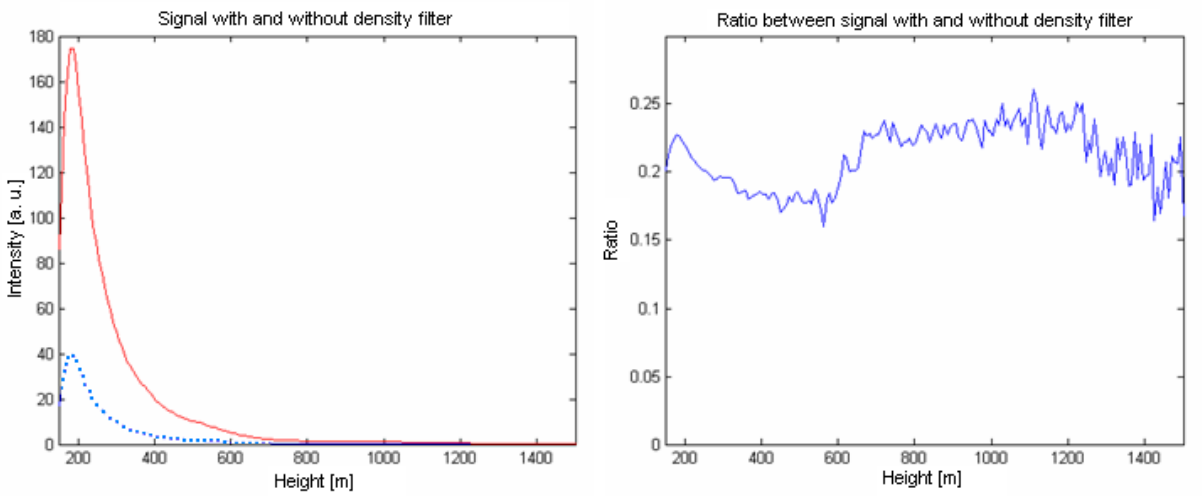


Fig. 1.4-9. To the left the signal from the detector with density filter in dotted line (blue) and without filter in solid line (red). To the right the ratio between the signal with and without is shown.

[10] The parts of the PMT and the function of these are described in section A.2 of the Appendix.

Fig. 1.4-9 above is describing the signal with and without filter, as well as the ratio between the same.

If saturation would have been present, the ratio between the signal with and without the attenuating filter should *increase* at the position of the strongest signal. This is not the case. Instead it seems as if the ratio instead is going in the opposite direction. This will be discussed more in section 1.5.4.

## 1.4.5. Averaging

When recording the lidar curves, a short laser pulse is sent out and the backscattering from this is sensed in the detector. Every second, twenty pulses are sent out and recorded. These pulses can either be analyzed one by one, or they can be *averaged*. When averaging is employed, a number of recordings are added together and the result is divided with that same number. In this way, more photons are used to obtain the signal, and the result therefore gets more reliable. The drawback is though that some of the time-resolution is lost. If twenty pulses are added to generate the signal, the time resolution is one second – in contrast to 50 ms as it is without averaging. Therefore there is always a tradeoff between time-resolution and signal-resolution in the choice of how many pulses to add up. Depending on the circumstances and the object that is to be studied, different choices are to prefer.

In this case, it is the movements within the atmosphere that are the main factors to take into account when choosing the averaging number. Since these movements are quite slow compared to the repetition rate of the laser, there is no point in having a too low number of averages. Only if quickly changing structures, like fast moving clouds are to be studied, the number should be set low. Lidar curves recorded with different number of averages, among others showing a cloud at a height of 3.7 km, are presented with two different amplifications in Figs 1.4-10 and 1.4-11.

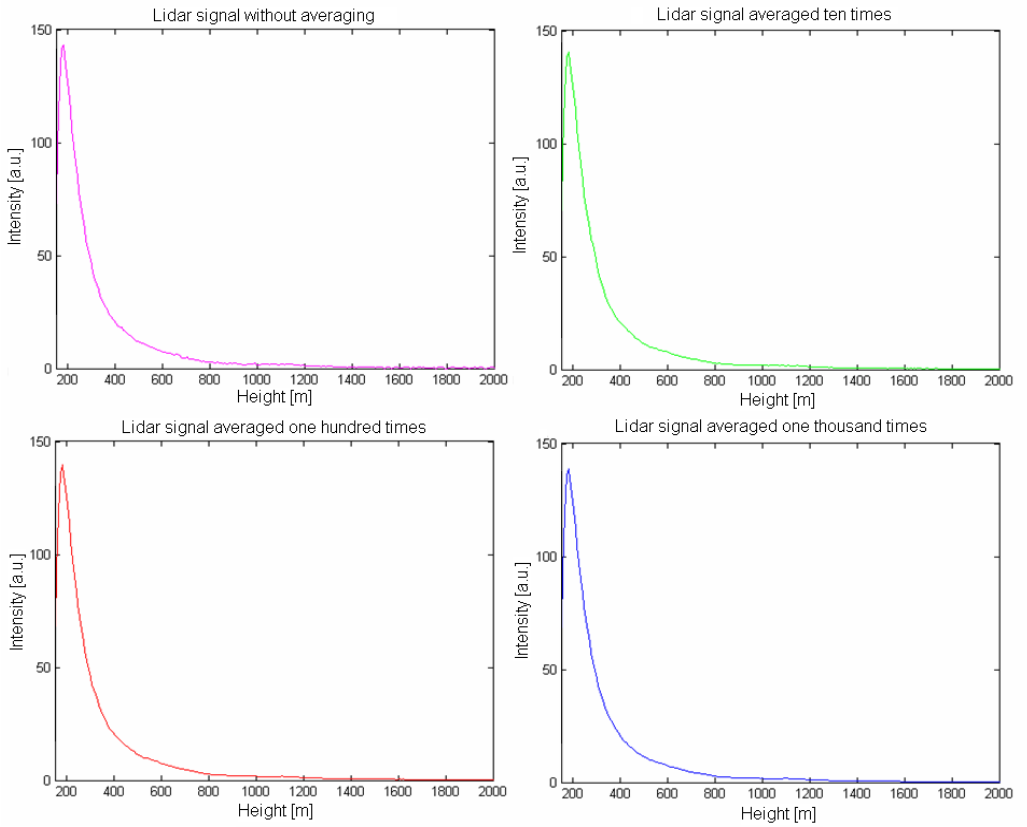


Fig. 1.4-10. Four raw lidar curves showing the effect of averaging. Top left: no averaging, top right: averaging 10 times, bottom left: averaging 100 times and bottom right: averaging 1000 times.

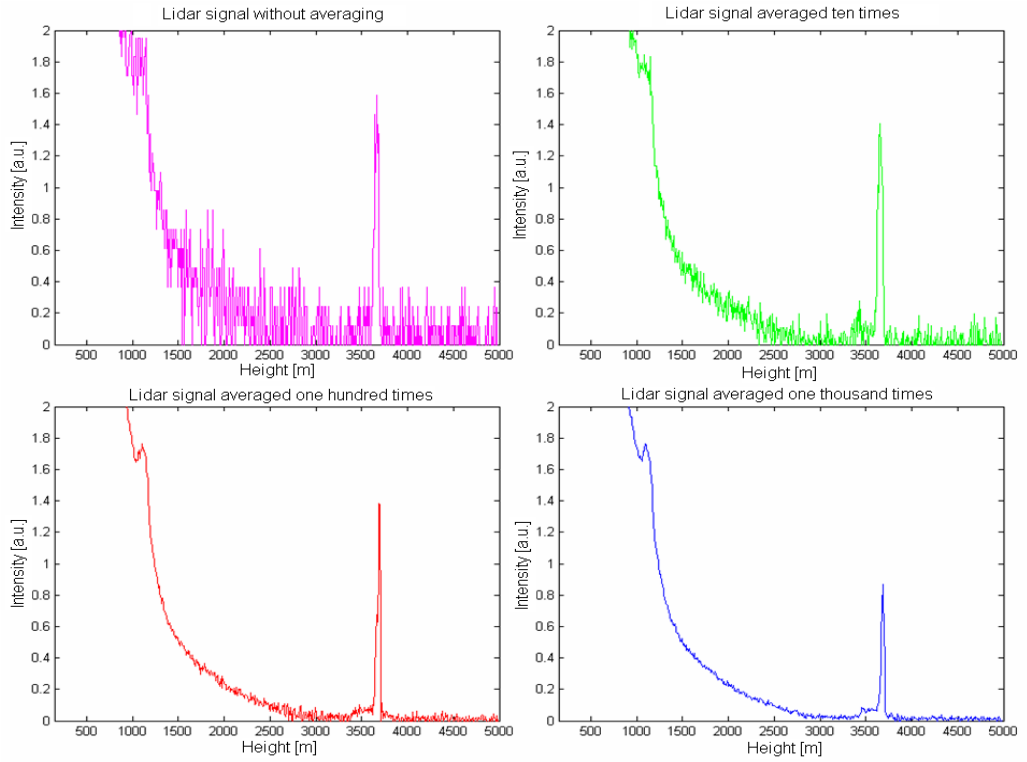


Fig. 1.4-11. Four magnified lidar curves showing the effect of averaging. Top left: no averaging, top right: averaging 10 times, bottom left: averaging 100 times and bottom right: averaging 1000 times.

## 1.4.6. Comparison with preliminary data from Hangzhou

As a continuation of the aerosol measurements performed in the rural location Vavihill in Sweden, comparative data were also obtained in a major Chinese city during November 2009. Hangzhou is a city with approximately 7 million habitants and consequently with a lot of traffic and large construction places but also with heavy industry. As this thesis is presented, the campaign in China is still going on and the data is not yet analyzed. However, some early lidar curves can be presented as a comparison to the ones obtained in Sweden. In Fig. 1.4-12, representative curves for clear weather are shown for the two locations. Data which were recorded during clear weather were chosen to exclude the impact of factors such as humidity as much as possible. The two curves have been normalized to each other with regards to their integrals.

The general behavior is that the solid curve (black), obtained in Hangzhou, is shifted towards shorter range compared to the curve obtained in Vavihill, shown in dash-dotted (red). In general, a shift of the lidar curve towards shorter range indicates more scattering. This is true in lidar cases with optically thin media and when single scattering is assumed. In other applications when multiple scattering is considered, the situation might be the complete opposite. For the curve from Hangzhou, the signal is strong in the beginning, indicating much scattering. However with distance, the signal from Vavihill is starting to compete and shows higher values after approximately 200 meters, as more light has been scattered away at this range in Hangzhou.

Most likely, the results show, as expected, that there are much more aerosol particles in the large Chinese city compared to the countryside of Sweden.

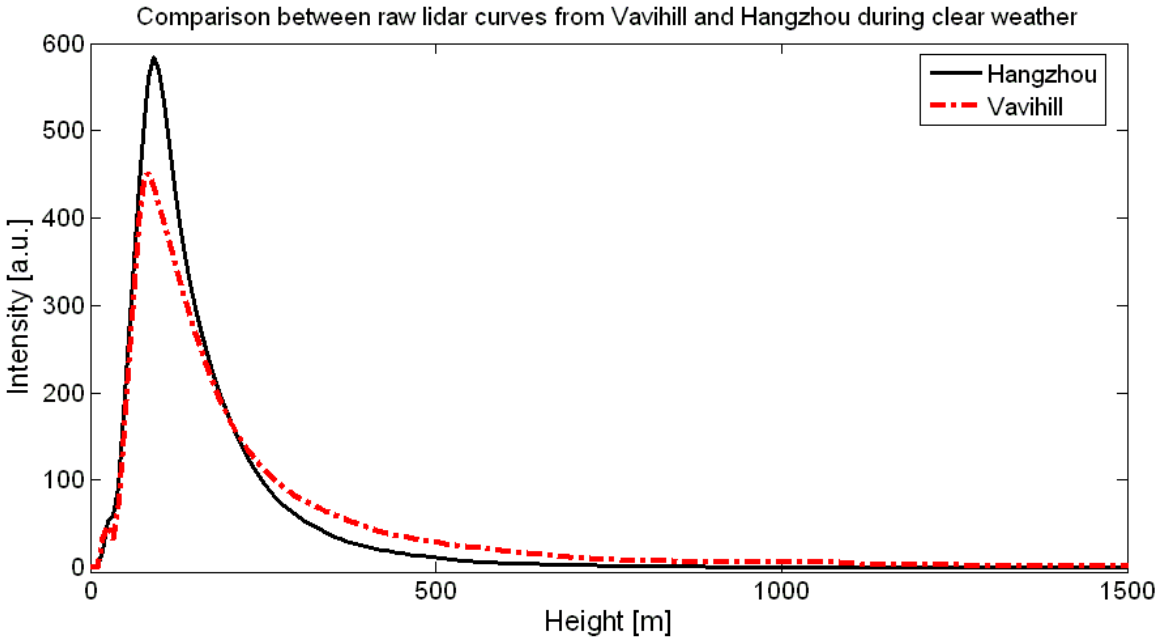


Fig. 1.4-12. Comparison between lidar curves obtained at Vavihill in Sweden and at Hangzhou in China.

# 1.5. Discussion

The four days in Vavihill were very fruitful and a lot of interesting results were attained. A lot of inspiring ideas arose through discussions during the campaign. Some of the ideas were also possible to realize directly and more are kept in mind for future work and will be discussed in the Outlook section below.

This campaign was as mentioned the first measurement with the Lund Lidar System with the purpose to study the structures of aerosols in the atmosphere. The hope is that this can be the starting point to more research within this very important field. The campaign can be considered as a trial where different measuring and analyzing methods were tested. During a future work, the methods have to be refined to get more reliable data and to provide more information about the atmosphere.

Discussed below are the results from the different parts of the campaign.

## 1.5.1. Aerosol particle distribution

### 1.5.1.1. The Fernald inversion method

A large part of the analysis of the data from the campaign was to calculate the scattering coefficient throughout the atmosphere. The question is then, how well can these results be trusted?

The exact numbers for the scattering coefficient in these results are based on the values from a nephelometer. This is as said placed at ground level, while the analyzed lidar data start to be reliable at around 200 - 300 meters. Obviously there is a gap in between that gives an uncertainty in the exact numbers. By comparing the results with what other groups have measured around the world, it although seems as if the values, at least, are in the correct order of magnitude.

The same goes for the *shape* of the curves obtained. Also these agree well to previous studies[11].

Generally, it can be seen that the aerosol concentration is higher close to the ground than at higher altitudes. This is usually what is found in aerosol measurements, with the low air typically containing more particles than the atmosphere above.

One thing that can be noticed in Figs 1.4-5 and 1.4-6 is an area with an increased scattering coefficient between around 1.0 and 1.5 km, especially visible during measurements on April 7 and 9. The increased scattering at these heights is implying a more dense area of aerosols. Very possible is that this region is the top (capping area) of the planetary boundary layer, which generally contains more aerosol particles than the surrounding air mass [32]. The altitude of this layer is as seen decreasing through the evening during the 7$^{th}$.

[11] Examples of studies are [23], [21] and [33].

The absolute values of the scattering coefficient are changing a lot over time during the campaign, not only the shape of the curves. As an example it can be noted that Fig. 1.4-3 shows a much higher scattering value in general than Fig. 1.4-1 and Fig. 1.4-2, especially for low altitudes. The background to this higher value is mainly a higher coefficient from the ground reference at this time. However, the calculated scattering coefficient drops quickly with height the first kilometer in this recording, implying that it is mainly the conditions at lower altitude which are changed. A possible reason for the suddenly much higher scattering at low height is that the humidity increased due to fog in the air. This recording was made at 20:20 on April 8 when it started to become dark and it is very possible that some "night fog" was recorded.

In Fig. 1.4-3, the scattering can be seen to increase at very high altitudes, around 6-7 kilometers. During the campaign, notes about the appearance of the sky were also made. Shortly after the time of this recording, a haze was seen around the visible moon and is probably what is seen as an increased scattering coefficient at around 6 km. Or, perhaps, the aerosols recorded by the lidar composed the base at which the haze could later form.

In the results obtained for the April 7 measurements, there can be seen an increased scattering coefficient both at around 1.5 and 3.5 km. During this day there was also seen by eye, both clouds and haze, while after 19:00 this was not the case. Comparing this to the data, it can be noted that after this time of the evening, less scattering is recorded at higher altitude. This implies that the clouds seen by eye are probably the reason for the increase in scattering coefficient at 3.5 km, while the layer at 1.5 km is more difficult to see by eye. Water droplets might have formed clouds around the higher particles but not, at least not to the same extent, on the lower ones.

At the start of the measurements on Wednesday the 8$^{th}$, the weather was cloudy which is also seen in the lidar data, showing a high scattering coefficient at around 1 - 2 km. At 14:20 the weather was noted as "clearer" while some areas of strong scattering can still be seen on the lidar data. This might imply that these are not due to water droplets, but rather other aerosol particles. At 17:15 the weather was considered to be "cloudy" and at 19:40 some haze was observed. This coincides well with the lidar data showing very strong scattering at 3 - 4 km between 17:00 and 19:30, approximately, and high altitude particles between somewhat before 20:00 to 20:30. In Fig. 1.5-1, the appearance of the sky is shown for two occasions during Tuesday, April 7 and Wednesday, April 8.


Fig. 1.5-1. Pictures taken of the sky at 18:12 on Tuesday the 7th and 19:14 on Wednesday the 8th. Both pictures show visible clouds, looking approximately the same. Lidar data shows that both these layers of clouds are situated at around 3500 meters altitude.

During Thursday the 9th, the weather was first noted to be "clear" during the morning but after 12:00, clouds came in and at around 13:00 the sky appeared to be covered by "thick clouds". This also correlates very well with the lidar data showing strong scattering at an altitude of around 1 km after 11:30. The clouds appear to have been so thick, attenuating the laser signal strongly, that the data above 1 km cannot be trusted. The data for the scattering coefficient show a clear atmosphere over this height, while it is not certain at all that this is the case. This in fact shows a limitation of the lidar method. One needs optical access to the area of interest and the structures above areas of dense cloud layers cannot be measured.

The discussion above is among others on the topic of the correlation between the scattering data and the appearance of the sky. This works as a way to make sure that the data are reasonable, but data of increased scattering are also seen when, e.g., no clouds were observed. This is implying that there are also a lot of aerosol structures which are not so easily seen by eye.

### 1.5.1.2. The Raman reference method

The hope was to also be able to use the nitrogen Raman lidar curves as references to obtain the profile of the scattering coefficient. Unfortunately, it turned out that the signal-to-noise ratio was not good enough to get high-quality results with this method. Still, this method is very straight forward and fewer calculations have to be done compared to with the rather complex Fernald method. If better Raman shifted lidar recordings can be done, the method is still promising.

The feeling of the author is that the Raman reference method, despite the "failure" in this first trial is the most promising to employ. When using this technique, one can be sure to have obtained a reference with the recording geometry exactly the same as for the curves to be analyzed. So if the method to record the Raman signal can be improved, and these recordings also can be done simultaneously to the elastic ones, this technique should surely work fine.

### 1.5.2. Depolarization

From the results of the depolarization experiment (see Fig. 1.4-7) it is clear that the polarization is changed more inside a dense cloud than in the surrounding air. By comparing the signals with polarization perpendicular to and parallel with the laser light, a value of the fraction of scattering events that change the polarization compared to those who do not, is obtained. This is generally entitled the *depolarization ratio*. At the position of the cloud, this ratio clearly goes up. However, the actual peak value of the ratio shown in the figure is quite sensitive to small altitude changes of the atmospheric layers between the recordings, so to obtain a more true value for the depolarization ratio, the integrated signal from the full cloud is compared between the two polarizations. In this way, a mean value of around 0.10 is obtained for the depolarization inside the cloud. Compared to the normal value to expect in air, which is around 0.04 [34], and which in fact corresponds well to the ratio at lower altitudes, it is therefore around two or three times as large.

As mentioned, there are mainly two possible reasons for the depolarization to be high; that the particles in the cloud are non-spherical or that multiple scattering occurs. Multiple scattering always occurs to a small extent but the probability for a photon to be scattered more than one time and still reach the detector is immensely small in normal air.

During the campaign, the outside temperature was around 10 °C at ground level. Generally, the temperature is decreased by around 0.65 degrees for every hundred meters increase in altitude which implies that the temperature at 1 km would be somewhat above 0 °C. But since these numbers are quite rough it is still possible that temperatures below zero were present at this altitude. Therefore the reason for the increased depolarization is still unclear.

One way to investigate if the depolarization is due to ice crystals or multiple scattering in a dense cloud would possibly be to observe how this ratio changes when the field of view of the telescope is changed. If the depolarization comes from multiple scattering, the depolarization ratio will increase when increasing the field of view, while this effect would not be as prominent in the case of ice crystals.

Interesting would also be to record the depolarization in a curve where two clouds, situated at different altitudes, are visible. At some cases, one cloud at around 1 km and one considerably higher were seen simultaneously. The depolarized signal is although quite weak, and the signal from the higher region would probably be too low with the polarizing cube set in the perpendicular mode.

It should be mentioned here that the general lidar equation presumes single scattering. This means that if a significant fraction of the scattering events are of multiple kinds, the lidar equation would be invalid. This is not a very big problem though, since this would only come into question in dense clouds, after which the lidar signal anyway is weak and difficult to analyze.

### 1.5.3. Impact of aperture size

First of all, it is required to mention that the results from this experiment are very dependent on the divergence of the beam. The qualitative results are general but the slope of the ratio is specific for the settings used.

The conclusions from the result of changing the aperture size might not be obvious. It was found that up until around 700 meters there was a difference between the signal strength from the measurements with the two aperture sizes. I.e., for distances less than 700 meters, the large aperture let more lidar signal through than the small one. One conclusion from this is that, since both apertures let equal amount of signal through in the range over 700 meters – both apertures let *all* light through here. If this would not be true, the large aperture would still have a stronger signal. Therefore the conclusion can be drawn that for both these apertures, no geometrical compression is present for distances more than 700 meters. By the same token it can be stated that 700 meters is the limit where the geometrical compression stops for the small aperture with the beam divergence used and that the limit lies at closer distance for the large aperture.

When observing Fig. 1.4-8, some prominent structures in the curve are visible. The reason for these is probably again that the measurements were not recorded simultaneously, and even if the effect of this was reduced by averaging many recordings, the structures are still there.

### 1.5.4. Saturation in the PMT

If saturation would have been present in the photomultiplier, an increase in the ratio between the signal with and without neutral density filter should have been visible. This was not the case. Instead, it seems as if the ratio declines in an area where saturation could be suspected. The reason for this decrease is somewhat unclear but is most likely changes in the atmosphere. The experiment shows that there are no indications for any saturation in the detector. There is neither any great reason to be doubtful when inspecting the specifications for the photomultiplier. But, since the shape of the recorded lidar curves are so essential in this application, it was important to make sure that no possible effects like this were present.

### 1.5.5. Averaging

In Fig. 1.4-10, which shows the large structures in a recording without any zooming of the figures, the effect of averaging is not very striking. This displays that the large structures of the lidar curve are clear even when only the backscattered photons from one single laser pulse are recorded. Of course, this conclusion applies only to the specific pulse energy, detection efficiency, etc., that were used.

In Fig. 1.4-11, on the other hand, where the signal from a cloud at an altitude of 3.7 km has been magnified, there is a clear difference between the curves. It is possible to see that a cloud is there without any averaging, but to see the structures of the cloud itself, it is necessary to average.

More importantly, to be able to calculate the scattering coefficient, or to do any other analyzing with the help of the lidar curves, the signal-to-noise ratio has to be sufficiently good. An averaging between 500 and 1000 pulses was therefore used in most cases during the campaign.

# Chapter 2 – Bird Monitoring

Birds, with their special advantage of being able to fly, can travel long distances in a relatively short period of time. This has made it possible for them to migrate and live at different habitats depending on season and in this way also to effectively spread genes. Every year, millions of birds travel thousands of kilometers, e.g., between Europe and Africa heading for seasonal breeding places.

Still, the seasonal habitats of different species of birds have not been completely mapped but this would be of great interest to get a more thorough picture of the global gene flow [3]. Birds are especially important in this aspect due to the large land areas they cover and travel. The spread of diseases is another central aspect, with the bird flue, which in the 90's was found also to spread to humans, as a striking example of the importance of bird migration research.

Questions that still are lacking complete answers are among others how, exactly, the times of travel are chosen, how the geography and winds affect the flights and, generally, how the habitats are selected and found year after year.

A number of remote sensing techniques for studying birds in flight have been developed and used. Examples are tracking radars, infrared cameras and ceilometers [3]. Observing flying birds at day time with binoculars of course provides important information. All these methods are though limited by different factors; unfortunately making it very difficult to distinguish between species, especially during night time when binoculars are impossible to use for this purpose. With radar, which is very effective in locating birds, a few species like the Common Swift (Sw. tornseglare), might be recognized with the help of their specific wing beat frequency [3], but this method cannot provide any classification help in the general case. The flying heights, which are often exceeding 1 km makes even visual classification difficult, even at daytime. The fact that many birds actually prefer to fly at nighttime thanks to beneficial conditions with, e.g., a less turbulent atmosphere and less risk of being caught by predators [3] makes bird classification at night time even more important.

Fluorescence lidar may provide a great contribution to the extra information needed to classify birds remotely. The fluorescence induced when the laser light hits the feathers of a bird is observed from a remote distance. Basically, the fluorescence gives information about the colour of a bird, and together with, e.g., radar, both the species and number of passing birds could be established.

In the corresponding section, test measurements both on a flock of flying Starlings and on museum samples of different species are presented as a means of classifying birds remotely.

# 2.1. Theory

## 2.1.1 Laser induced fluorescence

In a molecule, there are also vibrational and rotational energy levels, in addition to the electronic ones discussed in section 1.1.4. When this is taken into account, we end up with an energy diagram describing the possible energies that the molecule can have, schematically given in Fig. 2.1-1.

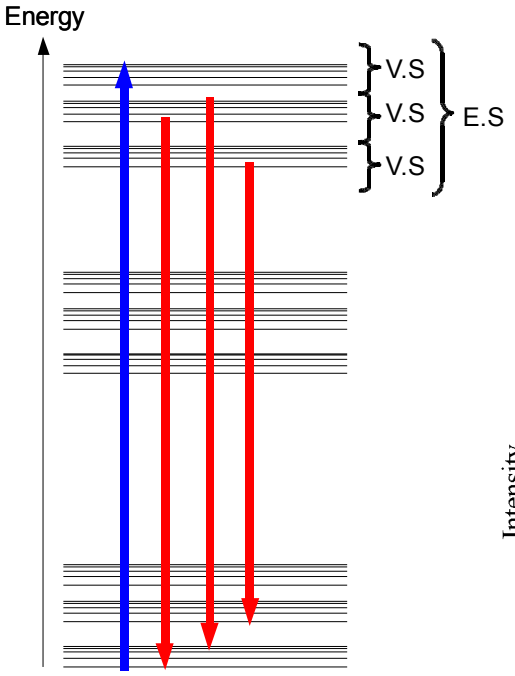


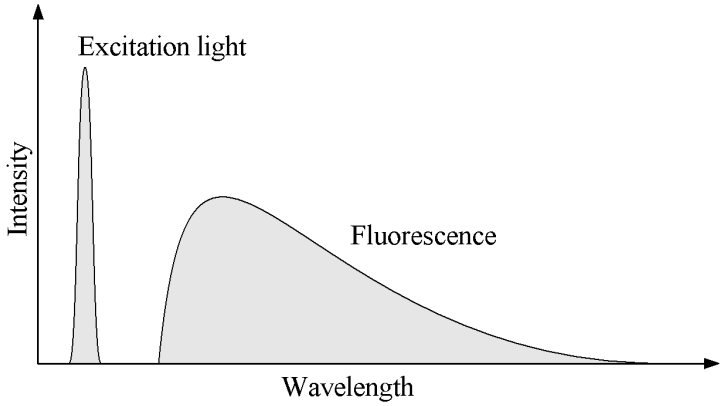


Figs 2.1-1 and 2.1-2. To the left: Fig. 2.1-1. Schematic energy diagram of a molecule and fluorescence. The largest groups of energy levels are belonging to the same electronic state, the smaller groups constitute vibrational states and each line is representing a single rotational level. The figure is not to scale. Below: Fig. 2.1-2. A general intensity distribution for fluorescence light as a function of wavelength.

Fig. 2.1-2 is illustrating how a molecule is excited by light with a short wavelength (typically UV light), represented by the blue arrow followed by fluorescence with less energy and thereby longer wavelength, in the figure represented by red arrows. The fluorescence can occur between a large number of sub-levels but typically, radiationless energy transfer puts the molecule in the lower part of the excited electronic level before the light is sent out. The radiationless energy loss occurs, e.g., in the form of heat generation transferred to surrounding molecules in a time scale of picoseconds while the fluorescence itself occurs in a time scale of nanoseconds [35].

If a laser is used as the excitation source and the fluorescence is studied, the technique is referred to as laser induced fluorescence (LIF), which is a very powerful probing technique, e.g., within the research of combustion processes.

The curve in Fig. 2.1-2 could vary widely depending on which molecule that is excited and on the wavelength of the excitation light. To completely describe the fluorescence from a certain object, the *excitation-emission matrix* (EEM) can be used. Here, the intensity distribution for the emitted light from a certain object is shown for every excitation wavelength. An example of such a matrix is given in Fig. 2.1-3.

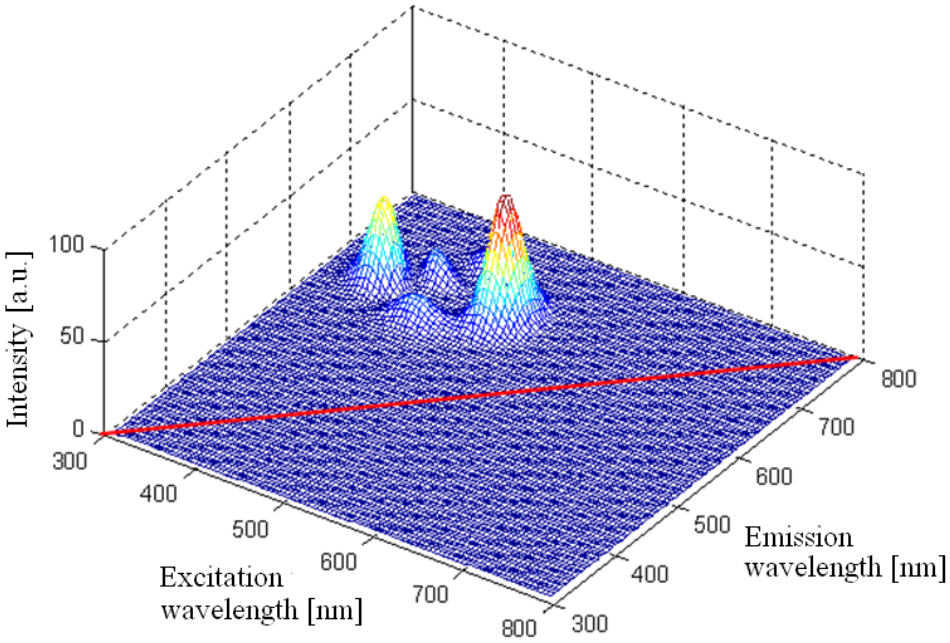


Fig. 2.1-3. Example of an excitation-emission matrix. The diagonal marked with a red line corresponds to elastic scattering where the emitted light has the same wavelength as the incoming one. Generally all structures will be on the low energy side of the diagonal, as the example shows. Only for special cases there can be light sent out with a shorter wavelength than the exciting one [3].

Elastic scattering or other resonant radiation, where the emitted or reflected light has the same wavelength as the exciting one will in this matrix end up on the diagonal marked in red. Generally, all fluorescence occurs on the low energy side of the diagonal where the emitted wavelength is longer than that of the excitation light.

## 2.1.2. Scattering and fluorescence from feathers

Birds have vision with four spectral channels compared to the three that humans have. One of the channels is positioned below 400 nm providing a UV band and the three remaining ones are in the same range of the spectrum as that of human vision; however, the exact positions are not the same. Considering this, it is not unlikely that the stunning variations in colour that humans experience when watching birds is even greater for the birds themselves.

The feathers on birds are, on a microscopic scale, hollow rather than solid. Incoming light will therefore most likely be scattered several times within the feathers before leaving the bird and reaching the observer. Most of the polarization and coherence information is therefore lost and the scattering is said to be incoherent.

The chemical properties of the constituents of the feather determine what wavelengths that will be absorbed, and therefore also partly what colour we will perceive for the bird. The

feathers are basically composed of a structure of β-keratine with chromophores[12] added [36]. The light absorption of the β-keratine itself is steadily increasing when going from 400 to 300 nm, and below 300 nm the absorption increases more rapidly. This molecule with its "dull" behavior cannot explain the sharp and beautiful colours observed in birds. Neither can the most common chromophores – eumelanin and pheomelanin, which give rise to dark and reddish colours, respectively. There are though some chromophores, e.g., carotenoids, which reveal sharper absorption features and therefore generate more characteristic colours [3].

The fluorescence which is induced in feathers by laser light is generated throughout a certain depth area. Thus, this "secondary" light will also experience absorption before reaching the observer. Because of this, the fluorescence is generally positively correlated with the reflectance, meaning that a bird that is reddish in reflectance is likely to be reddish also in fluorescence [3]. However, this is not always the case.

### 2.1.3. Interference effects and structural colours

Structural colours arise from light *interference* phenomena. Common is that the interference takes place at the surface of a material with a layered structure. Interference of light can occur when two or more light waves are reflected at different depths in this material, or if a single light wave is partly reflected at two different positions[13]. Depending on the difference in pathway that the two light waves experience, either constructive or destructive interference can take place, or anything in between. The principle is shown in Fig. 2.1-4.

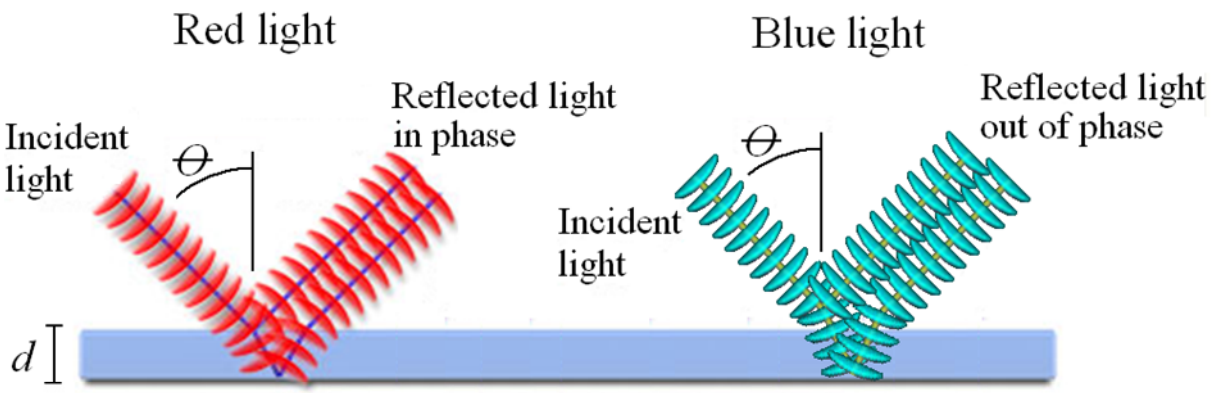


Fig. 2.1-4. The principle of interference in a thin film or a general layered structure.

If the two reflected light waves are in phase, they can interfere constructively and in the contrary case, when they are completely out of phase, the interference is destructive. When constructive interference occurs (in reflection), the amplitudes of the two reflected waves are

[12] A chromophore is the part of a molecule which is responsible for its colour. The chromophore thus has an internal energy structure which falls within the visible spectrum.

[13] It is vague to talk about a single or several light waves. This description is purely pedagogic but for further investigation more thorough theories have to be used.

added in each point, and the reflection will be strong. If destructive interference takes place on the other hand, the amplitudes will be subtracted from each other, and no light might be reflected. In this example, the wavelength of the red light matches perfectly the thickness, $d$, and the angle, $\theta$, so that the reflected light is in phase. For the blue light on the contrary side, the wavelength is shorter and the reflected light is out of phase. This strongly influences the perceived colour.

As the interference depends on how the difference in path length between the individual reflected waves matches the wavelength of the light, it also depends on the incident angle, $\theta$, and the refractive index of the medium. If light consisting of many colours, i.e. with a broad spectrum, is illuminating an object with this property, the different colours will be preferably reflected in different angles. In this way, objects with structural colours tend to have different hues depending on the angle of viewing.

An example of this is the neck of a pigeon, where a rainbow-like colouring can be seen.

The structures which are responsible for the interference layers can in the biological world be, e.g., small "nano-spheres" just below the surface of the material. These nano-spheres have a size in the order of 100 nm, effectively interfering with visible light, having a wavelength of about 400 – 700 nm. Also thin layers of wax or oil can create the same effects through thin-film interference. The latter is frequently observed in bird colouration [3].

These phenomena will give additional effects to the "normal" colours arising from the selective absorption of light with different wavelengths, which is how most colours in our environment are created.

## 2.2. Laboratory work

As a complement to and help for the lidar measurements, indoor point measurements were performed on the 24 museum birds. The measurements were performed by Mikkel Brydegaard in connection with the lidar measurements described. Selected spots were alternately illuminated with 255 nm and 355 nm radiation from light emitting diode sources. Both the diffuse and specular reflections and the fluorescence were collected and analyzed with a spectrometer.

The results from selected bird feathers are presented in a logarithmic scale for 355 and 255 nm illumination in Fig. 2.2-1 and 2.2-2, respectively. The spectrometer is not white light calibrated.

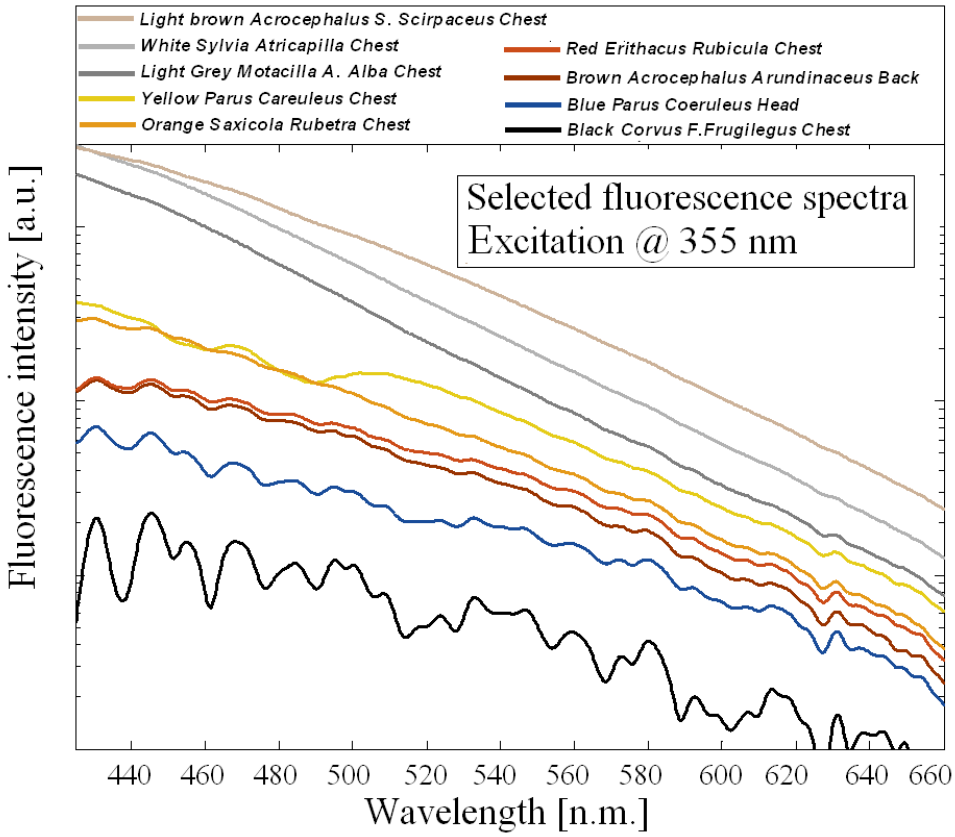


Fig 2.2-1. Selected point fluorescence spectra with illumination at 355 nm. The legend names are ordered as the intensities are (starting from the highest) at 550 nm. Modified from [3].

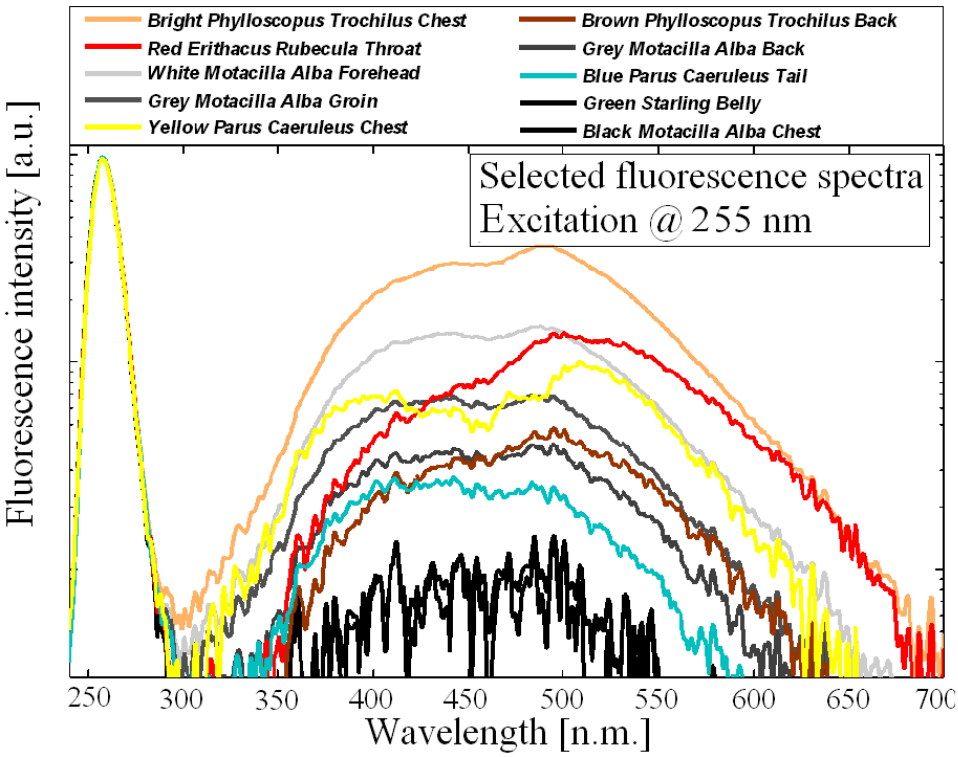


Fig 2.2-2. Selected point fluorescence spectra with illumination at 255 nm. The legend names are ordered as the intensities are (starting with the highest) at 550 nm. Modified from [3].

For the 355 nm illumination, it can be seen that the spectra corresponding to grey and white feathers show the same shape, although with different absolute intensities. This goes well together with the reflection case (the colours that we perceive for the birds). Also the fluorescence for the redder samples (red, brown and orange) is similar to what is expected for reflectance, as the relative intensity at longer wavelengths are higher for them compared with, e.g., white samples. With this argumentation, the spectral behavior for the blue feather should be the opposite, which is not the case. However, here the situation is a little bit different. First of all, the over all fluorescence is very weak making the result difficult to interpret. This indicates both that the reflectance at 355 nm is strong and that the fluorescence yield is low. Another difference is that, at least partly, the blue colour on this feather is generated structurally. Still, we conclude that the fluorescence from the blue feather is not positively correlated with the reflectance.

It can also be observed that there is a characteristic double dip in intensity (or double peak in absorption) for the yellow feather of the Blue Tit (Sw. blåmes). This arises from the spectral properties of the yellow carotenoid which absorbs or quenches some of the fluorescent light [3].

The fluorescence measurements with 255 nm excitation show, as for 355 nm illumination, that white, grey and black plumage maintains the same shapes but with different intensities. Brown and reddish feathers are shifted towards the red. Also here the double dip in the yellow feather is observable and so is the low fluorescence from the blue feather of the Blue Tit.

## 2.3. Experimental setup

The measurements were in fact performed in connection with studies on damselflies [37]. As the study on these insects actually laid the foundation for the bird experiments and is the reason for the chosen spot, a short section introducing this subject is provided in the Appendix, section A5.

The basic system used in the field experiments was the same as in the aerosol campaign in Vavihill. In this campaign, the lidar truck was parked on a dirt road (see Fig. A.5-2) close to the river *Klingavälsån*. In between the truck and the river, there was a field, about 100 meters wide. The laser beam was sent out across the field to the river around which the birds were flying. When the light fell onto a bird, the reflected, elastic signal was recorded in one channel together with the fluorescence in two other colour channels. The basic setup is shown in Fig. 2.3-1.

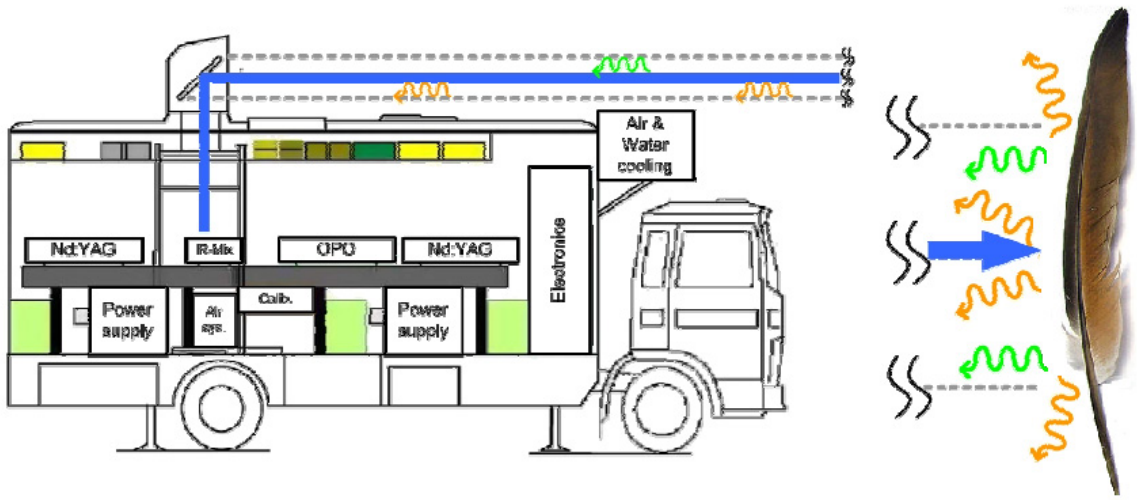


Fig. 2.3-1. Schematic illustration of the stimulation and recording of fluorescence from the surface of birds with the lidar system. Modified from [37].

The fluorescence should, as described in the theory section, be used to distinguish between different species of birds and therefore provide extra information. Also, to record in three channels simultaneously, as was done, provides an extra level of insurance that the signal is "real". If a "fake" signal, due to, e.g., electronic errors would appear, it is most unlikely that this would happen in three channels at the same time. Details about the multi-channel system will be given in section 2.4.

Again, one of the Nd:YAG lasers produced light pulses at 355 nm, which were sent out via the expander, folding mirror and quartz window.

Normally, a transient digitizer is used to read out the signal from the detector. This is especially developed for lidar, and has several advantages that will not be discussed here, but for this purpose, an oscilloscope was instead used to read out the signal. The reasons for this are mainly two; the sampling rate of the oscilloscope is very fast, so the range resolution can be good, and it also has the possibility to record three different channels simultaneously, which is crucial for this purpose. During the experiments, a sampling rate of 125 MHz was used, resulting in a range resolution of around 2 - 3 meters.

## 2.4. Additional equipment

An important new piece of equipment was used to attain a multi-channel detection scheme. The new scheme was developed after the vertically sounding aerosol campaign to be able to record not only one channel of light, which, e.g., would be the elastic, but also two fluorescence bands (or the Raman shifted signal, another polarization, etc., in the aerosol case). In Fig. 2.4-1, a schematic diagram is presenting the design of this PMT setup.

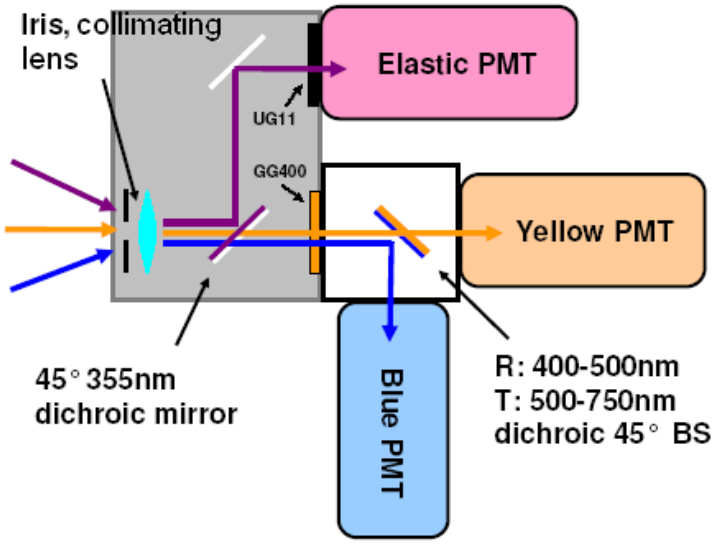


Fig. 2.4-1. Multi-channel detection PMT setup. Modified from [37].

A dichroic mirror, with a high reflectance for 355 nm but transparent for longer wavelengths, is placed after the iris in an angle of 45 degrees. The elastic light will thereby be directed towards one PMT ("Elastic PMT") via a secondary mirror. The fluorescence is transmitted and passes through a long-pass-filter (GG 400), assuring that no elastic light is left. A dichroic beam-splitter then separates the fluorescence into two PMT's; one for light with wavelength shorter than 500 nm ("Blue PMT") and one for light with wavelengths between 500 and 750 nm ("Yellow PMT").

The first measurements on birds were performed with the laser wavelength 355 nm. Since this wavelength is not completely eye safe for birds, a lower wavelength, e.g., the 4$^{th}$ harmonic of the Nd:YAG laser at 266 nm, should be used in a future application. To further explore this possibility, this wavelength was also used as an excitation source during tests in a laboratory environment. 266 nm light is completely eye safe for all animals [3]. This first bird fluorescence project was as stated conceived in connection with a damselfly monitoring project where accidental bird hits did occur.

## 2.5. Measurements and results

### 2.5.1. Measurements done *in situ*

To explore the feasibility of using lidar to find and separate different species of birds, recordings were done in the field, both on live birds and museum specimens. Live Starlings were incidentally caught in flight at a short distance.

Fig. 2.5-1 shows an example of a lidar return signal from a flying Starling, obtained in a distance of approximately 85 meters. The signal is time/distance resolved in one elastic reflectance channel at 355 nm, one fluorescence channel ranging from 400 to 500 nm, henceforth denoted "blue" fluorescence and one channel ranging from 500 to 750 nm, denoted "yellow" fluorescence.

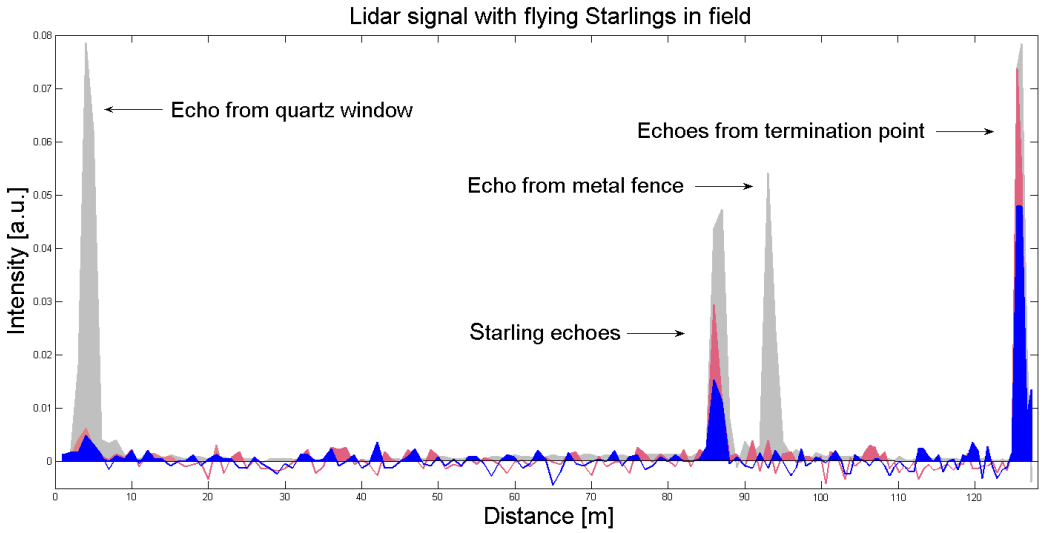


Fig. 2.5-1. Three channel time resolved lidar signal showing echoes from the quartz window, a bird, a metal fence and a termination point.

Included in Fig. 2.5-1 are the return echoes from the quartz window, from the bird, from the metal fence and from the termination point where the laser beam is hitting ground. The signals are strong in all three channels at the distance of the termination and these signals are also used to obtain the results shown in Fig. 2.5-3, but to clearer demonstrate the echoes from the bird, the termination is excluded in Fig. 2.5-2.

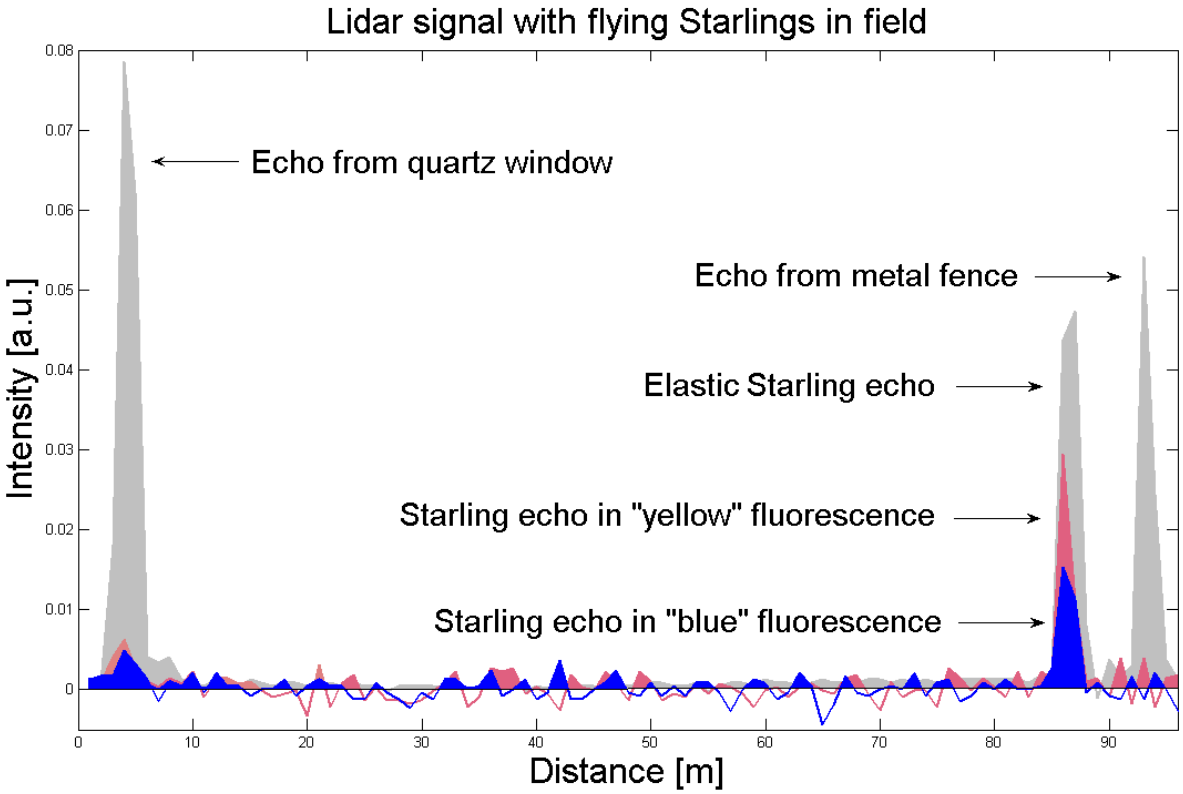


Fig. 2.5-2. Magnified version of Fig. 2.5-1, showing the echoes from the bird clearer.

The reflection from the quartz window in the light pathway is clearly seen in the elastic channel, while almost no fluorescence is indicated here. This shows that any potential leakage between the elastic and the fluorescence channels is in that case small. At a distance of around 85 meters, all three channels give strong signals, showing that not only reflection is present, but also fluorescence in both the blue and yellow range. Direct comparison between channels is however not meaningful since the detection efficiency differs between the detectors. Shortly after 90 meters, the elastic reflection from wires of a non-fluorescent metal fence is seen.

The possibility to distinguish between different species with lidar was further investigated by recording the return signal in a similar way as for the live Starlings, but for the museum birds specimens investigated with laboratory point measurements. The specimens were each put in and out of the light pathway at the position of the live Starlings echoes to simulate birds flying into the beam.

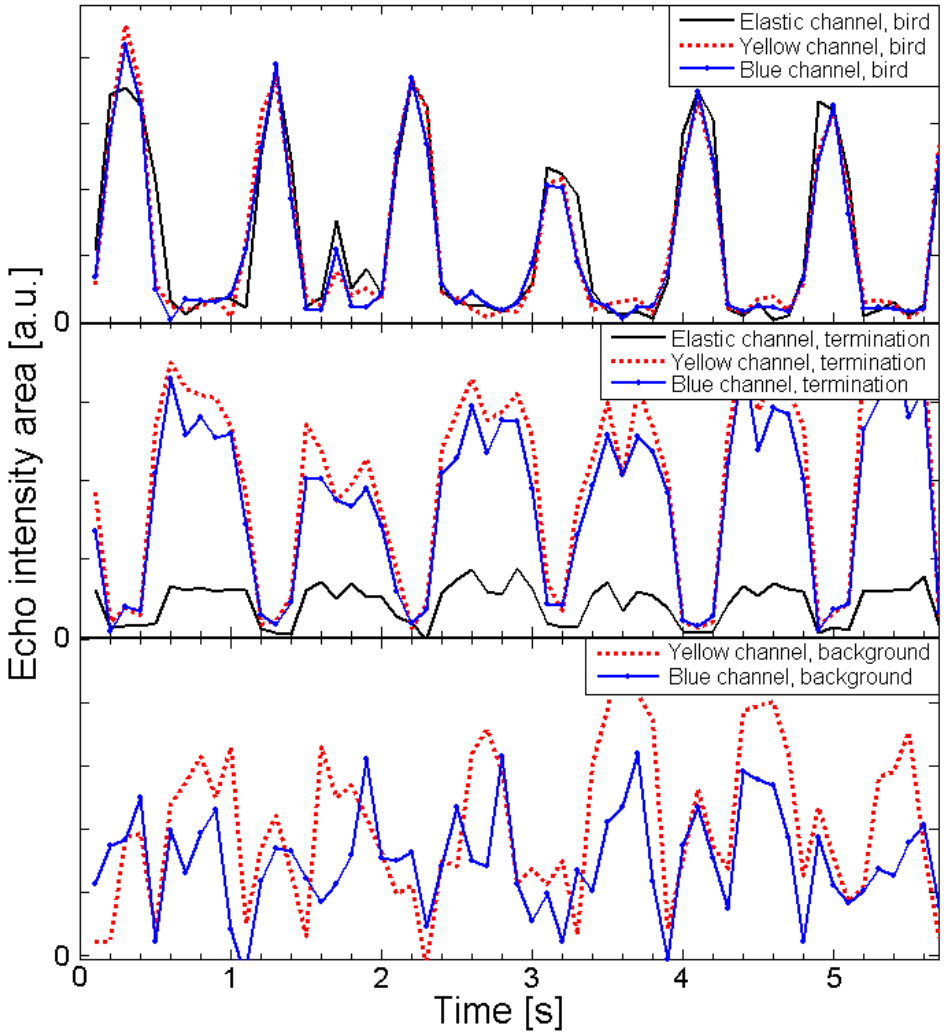


Fig. 2.5-3. The echo intensity area as a function of time for the signals from a bird, from the termination echo and from the integrated background light. The variations in the signals come from that the bird is put in and out of the beam in an oscillating manner.

Fig. 2.5-3 shows an image of a time period over which a museum bird was put in and out of the beam in a cyclic manner. In all sub-figures, elastic signals are shown in black, fluorescence between 400 and 500 nm in blue and fluorescence between 500 and 750 nm in red. The top sub-figure shows the integrated total returning light from the distance where the bird is inserted as a function of time for the three channels[14]. As the bird is moved into the beam, all channels show increasing signals at the corresponding distance. At the same time, both the elastic signal from the metal fence and the signals from all channels at the position of the termination go down. This is exemplified in the middle sub-figure of Fig. 2.5-3, which shows the behavior of a similar intensity area as for the birds, but now for the position of the termination point.

It might be worth to note here the close connection between this approach – to observe how the signal from a remote object is obscured by a closer one – to that used within astronomy. To monitor how the light intensity from a distant star is suddenly decreased when a darker object passes is a very useful method to discover exoplanets in other solar systems.

Since the intensities at the detectors which correspond to both these distances are induced by the laser light, the observation of these is active monitoring. But another thing can in fact also be observed when the bird is moved in and out of the beam path. The background light that reaches the detector also goes down. This is shown in the lowest sub-figure of Fig. 2.5-3, where the signals at the two fluorescence channels go down synchronized with the increase of bird fluorescence. The background light is obtained by summing the intensity for all light that reaches the detector after the backscattered light from the termination has done so. When this termination light has returned, the laser pulse is no longer present and all light that reaches the detector from now on comes from other sources (the Sun).

As for the classification of different species with the help of the fluorescence light, the procedure is that the intensity area (basically the strength of the echo) in each channel is recorded for every laser pulse that gives a signal. The values in each channel are then presented as a small mark in a scatter plot where the axes are chosen to achieve the best separation between species of interest. One result of this is Fig. 2.5-4 which shows such a plot for museum samples of a Robin (*Erithacus r. rubecula*, Sw. Rödhake), a Blue Tit (*Parus careuleus*, Sw. Blåmes), a European Reed Warbler (*Acrocephalus s. scirpaceus*, Sw. Rörsångare), a Starling (*Sturnus v. vulgaris*, Sw. Stare) and a Jackdaw (*Corvus monedula*, Sw. Kaja). The illumination wavelength is 355 nm.

[14] That not only a single peak value at the distance of the bird is used is to give a more accurate value of the actual power of the reflectance/fluorescence. The exact height of the peak depends on how well a single electronic sampling occasion in the detection coincides with the strongest signal. To instead observe the area under a peak (as the filled peaks in Fig. 2.5-1 indicate), gives a much better estimate of the true properties.

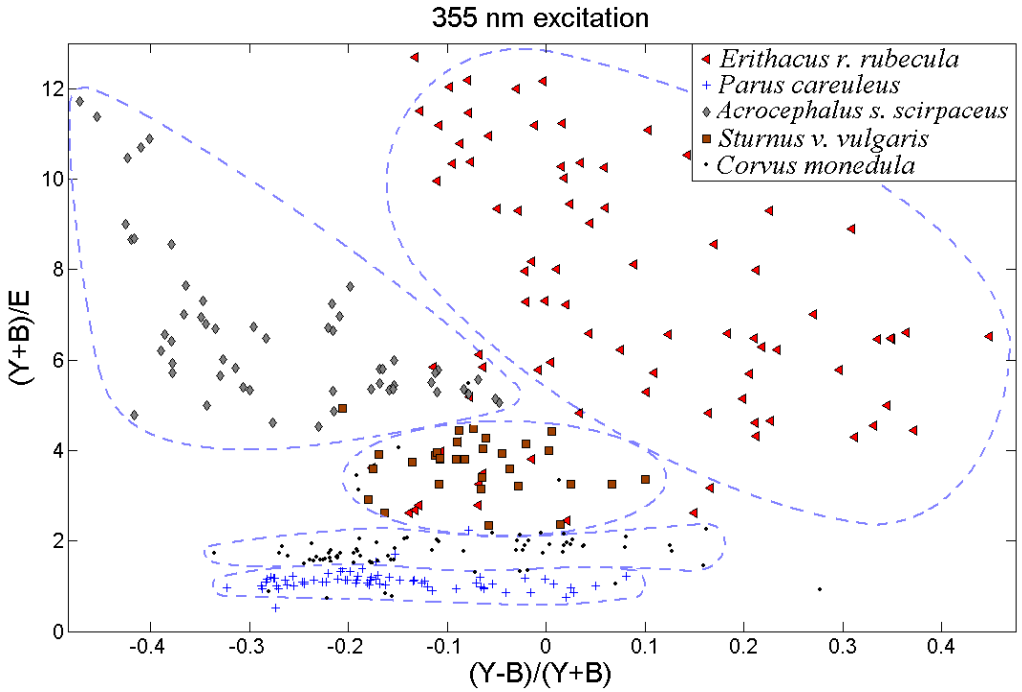


Fig 2.5-4. Scatter plot of five museum birds of different species. The axes in the figure have been chosen to maximize the separation of the species. Capital Y stands for fluorescence in the "yellow" channel, B stands for fluorescence in the "blue" channel and E for elastic light. The y-axis is thus a measure on how strong the total fluorescence is compared to the elastic signal and the x-axis is a measure of the shift towards red in the fluorescence light. Both axes are unit less. Dashed demarcation lines are drawn for the guidance of the eye.

## 2.5.2. Complementary measurements

As a future ambition is to use shorter wavelengths than 355 nm as excitation for the LIF measurements on flying birds, this possibility was evaluated in the lidar mode from the docking position of the lidar system in Lund. The wavelength corresponding to the fourth harmonic of the Nd:YAG laser[15], 266 nm, was used to illuminate the same museum birds that were also used in field measurements with 355 nm light. The birds were, in the same way as during the field experiments, placed in the laser beam, but now on the top of a roof, as seen in Fig. 2.5-5.

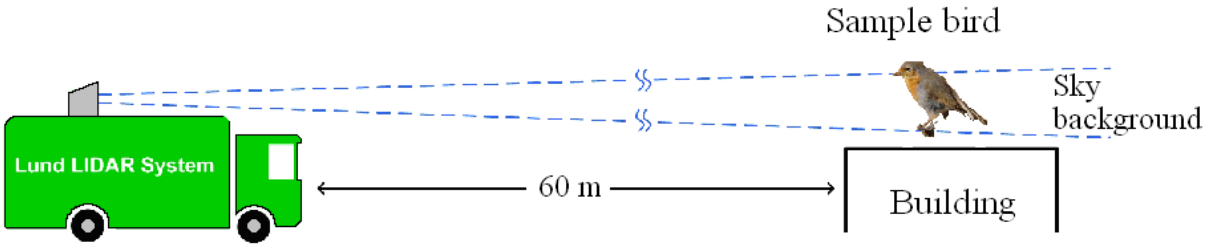


Fig. 2.5-5. Schematic setup for roof-top measurements on museum birds with 266 nm illumination [Modified from [37].

[15] In this particular case, this wavelength was however generated with the optical parametric oscillator of the lidar system.

Scatter plot results from the measurements with 266 nm light on a Great Reed Warbler (*Acrocephalus arundinaceus*, Sw. Trastsångare), a Black Cap (*Sylvia atricapilla*, Sw. Svarthätta), a Starling (*Sturnus v. vulgaris*, Sw. Stare) and a Rook (*Corvus f. frugilegus*, Sw. Råka) are shown in Fig. 2.5-6.

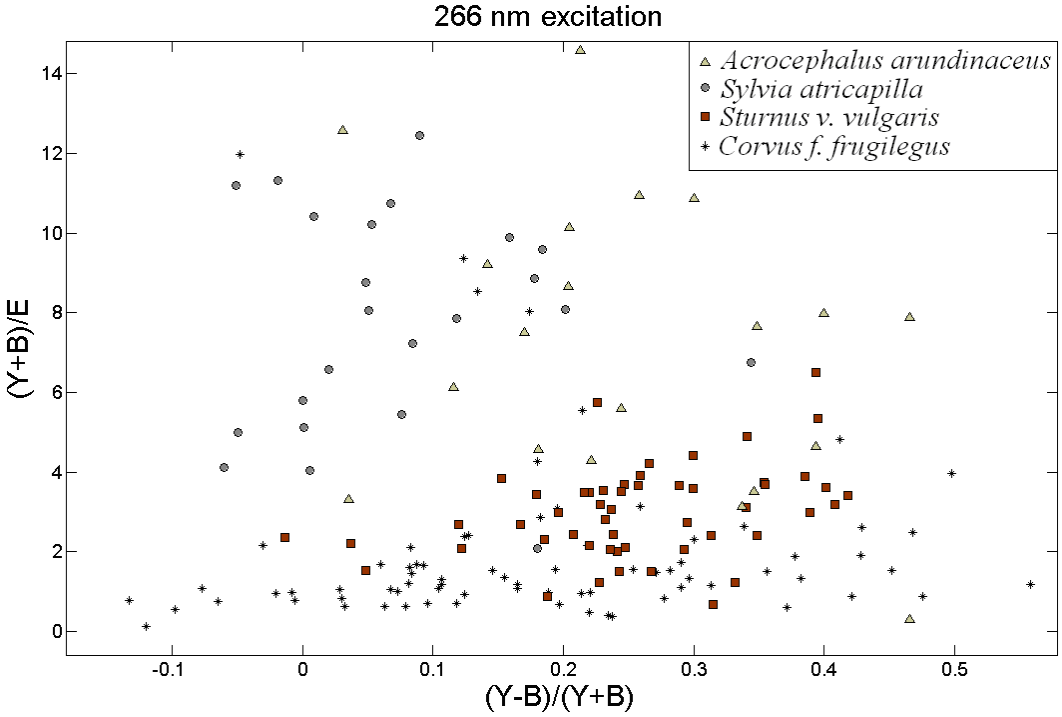


Fig 2.5-6. Scatter plot of the fluorescence from four museum birds of different species held at a roof top in Lund and illuminated with 266 nm laser light. The axes are the same as in Fig. 2.5-4.

# 2.6. Discussion

## 2.6.1. Measurements done *in situ*

The idea of collecting the fluorescence in more than one colour band is, as explained, to be able to separate species with the help of their different fluorescence spectra. To do this, the strengths of the fluorescence in the different bands are compared with each other. But in this way, a bright colour gives the same ratio as a dark one with the same hue. To provide more information we would also like to know how strong the total fluorescence is from the bird. For this information to be useful we also need to know how much excitation light that actually illuminated the bird – the bird-beam overlap. What has been done so far to obtain the results presented, is that the sum of the fluorescence has been compared to the elastic backscattering (the y-axes of the scatter-plots). As the strength of the backscattering of course depends on how much light that illuminated the bird, this does the job reasonably well. But one should bear in mind that the amount of backscattered light also depends on the reflection properties, which also varies between species. It is therefore not clear that a lighter bird should show a larger ratio between fluorescence and elastic reflection than a dark one.

In Fig. 2.5-3, another possible way to calibrate the fluorescence has been examined where the intensity from the termination point and background level have been observed simultaneously with the signal from the bird. As the signal from the termination point varies accordingly to the signal from the birds, but in the opposite direction, this shows that the bird obscures an essential part of the beam. A possible substitute for the termination point that can be used in the vertical mode, would for example be the base of a thick cloud.

Another possibility which perhaps is the most promising one would be to use the total elastic backscattering signal from the atmosphere, summed over an extensive range above the bird – essentially the same signal as is discussed in Chap. 1. If the integrated atmospheric backscattering signal is compared for pulses just before the bird was seen, and the pulse/pulses that hit it, a very good measure on the bird-beam overlap would be obtained.

Also the background light level apparently varies as the bird is obstructing the field of view, although not as obviously. This information may thus provide an alternative way of inactive calibration instead of using the elastic backscattering as a reference. But to perform well, the technique has to be further improved. One advantage with this method is that one less detection channel is needed.

That the intensity at the detectors from the background light goes down when the bird is inserted in the beam is in fact not self-evident. As less light is reaching the detector when the bird is in the telescopes field of view, this area must now be darker than without the bird there. If a really dark termination is used and a white bird is flying through the beam, this background level would instead increase. However, in the vertical mode, with the sky as background, the case presented here is perhaps the most probable.

The scatter plot in Fig. 2.5-4 shows promising results, indicating that it in fact is possible to separate different species of birds with the help of a multi-channel fluorescence lidar system. The five different species of birds tend to gather at different positions in the plot, showing the variation in fluorescence between them. The Robin which has a clear red belly tends to go to the right side of the plot and also shows a relatively strong fluorescence compared to the other birds. Another species that fluoresces much is the European Reed Warbler which on the other hand has a hue more shifted towards the blue. In the centre of the plot, the points from the somewhat darker Starling gather with less strong fluorescence. The fluorescence colour is as expected peaking between the red robin and the more grayish reed warbler. The Jackdaw also shows a low fluorescence which corresponds well to the fact that it is dark grey or black. What might at the first glance be very surprising is that the Blue Tit shows even lower ratios between fluorescence and elastic light than the black bird. There is though an explanation for this as revealed by the laboratory point measurements. First of all, the Blue Tit turns out to reflect light very well at this wavelength [3]. The outcome of this is that the denominator in the y-axis is increased (the fluorescence is normalized to the strength of the reflection) while

at the same time the numerator is decreased – since the reflection is strong there is little light left to generate fluorescence. The fluorescence yield[16] might also be low.

Photos taken of the same bird specimen that are discussed here can be found in the Appendix, section A.4.

## 2.6.2. Complementary measurements

The measurements performed with 266 nm light were done with a much lower output power of the laser than the ones with 355 nm light. This fact and others made the signals weaker and the resulting scatter plot is not as clear as the one for 355 nm. Still, some separation can be distinguished in the backscattered fluorescence. As an example, the black Rook shows low fluorescence, the relatively dark Starling a bit more while the brighter Black Cap and Great Reed Warbler fluoresce more. One might also be able to discern that the Black Cap is more shifted to the blue than the Great Reed Warbler. Also the photos of these birds can be found in section A.4 for comparison.

The technique clearly needs to be refined before reliable bird identification can be performed independently. The scatter plots show results that can provide help to separate species if previous insights already exist, offering only a limited number of species to choose from. As the plots are only considering four and five species and still some overlap is seen, it would clearly be impossible without improvements to separate between a greater number of arbitrary bird breeds. At this stage, much assistance from other techniques, like radar, IR imaging or general knowledge is needed to provide the desired results.

Also worth mentioning is that the distance to the investigated sample birds was relatively short compared to the general real-life situation. So would the results then be much worse in a situation with a flock of bird passing at an altitude of, say one kilometer? The apparent answer would of course be yes, but that might not be completely true. Firstly, the system can relatively easily be converted to output more light, which directly improves the signal quality. With a voltage ramped PMT operation, the signal at long range can actually be improved to compete with the close range signal, compensating slightly for the obvious geometric signal loss. The flying bird would also, at least in part of its wing cycle have a much larger target area, also refining the signal, and finally, as discussed in Chap. 1, vertical sounding, which is the preferred mode of operation in this case, always provides much better signal quality. All this combined makes the fluorescence lidar technique a very possible help in the quest to detect and distinguish bird species at normal flying heights.

[16] The fluorescence yield measures how much fluorescence that is generated from a certain amount of absorbed light.

# Outlook

## O.1. Aerosol measurements

As mentioned, ideas for future experiments are at hand regarding vertical aerosol monitoring. Examples of fascinating research to perform are among others the use of multiple, simultaneous recording detectors and multi-wavelength transmission. Both these opportunities will be discussed below.

Several of the experiments performed had the purpose to compare different recordings with each other: vertical recordings with horizontal, recordings with window and without, recordings with different aperture sizes, recordings of light with different polarizations, etc. To be able to compare all these things, it is clearly an advantage to do it for the exact same properties of the sky. The best way to do this is to perform simultaneous investigations – to record the curves to be compared for the same laser pulses. In some of the cases, this was anyway not possible; the vertical measurements could not have been done with the same laser pulses as the horizontal ones, nor could the recordings with and without window. But a good example of an experiment that would have benefited from simultaneous recording is the measurement of different polarizations. Another is the Raman signal compared to the elastic one. In both these cases, a multiple detector setup with beam splitters or dichroic mirrors could have been used to simplify the analyzing process. The opportunity to do this kind of recordings was though made possible shortly after the corresponding campaign, through the new design of a multiple detector scheme, which actually formed the basis for the work in Chap. 2. We are looking forward to use this advantage in future campaigns.

Another promising mode of operation that could be used in future campaigns is to use multiple colours or wavelengths of the laser pulses. This can provide much important information, especially about the particle size distribution of aerosols. During the campaign presented here, the third harmonic of the Nd:YAG laser at 355 nm was used. There is however the possibility to use light of other wavelengths, also multiple ones simultaneously. The optical parametric oscillator (OPO) in the Lund Lidar System can provide light of a wide wavelength interval, ranging from around 220 nm to 1.7 μm. There is also the possibility to use the second harmonic and fundamental frequency of the Nd:YAG, at 532 and 1064 nm. However, if longer wavelengths than 355 nm should be used, there are increased safety aspects to bear in mind. The cornea and lens of the eye are highly absorbing in deep-UV but also to a strong extent around 355 nm. Therefore it is more difficult for light with a short wavelength to reach the retina where it can do most damage. This is not the case for the visible, e.g., 532 nm, and infrared, 1064 nm, light. The eye can focus this light and these wavelengths are therefore much more dangerous.

With proper safety precautions, it is still promising to employ multiple wavelength lidar to obtain more information.

As stated, during the presentation of this thesis, the same type of measurements as performed in Vavihill are performed with the Lund Lidar System in the east part of China and a comparison between the results obtained in Sweden and in Hangzhou will form the basis for interesting future work. Hopefully, the aerosol structure can also be obtained at other locations.

## O.2. Bird monitoring

The work of studying birds and possibly also other animals with laser induced fluorescence is still in a very early stage and much effort will be put into improving the technique and the possibility of usage in a real *in situ* situation. Investigations will hopefully be done on the opportunities to use the technique also on for example night moths and bats during the beginning of 2010.

The three channel system that was integrated for the LIF measurements could very well be extended to have more detectors. In this way, there will basically be more dimensions that can be used in the analysis and the possibility of distinguishing between species might increase. This is one possible way to improve the method. However, as the fluorescence spectra of the birds are quite structure-less (at least in most cases) there is no point in having a too large number of recording bands. No additional information will anyway be obtained.

The driving force behind the development comes, to a very large extent from ecologists already involved in the field. During the spring and summer of 2010, vertical measurements are planned on flying birds in a live situation. There are locations in Sweden where a large number of birds pass during certain time periods; e.g., Falsterbo and the south tip of Öland, during the autumn migration south and Kullaberg during the spring-time migration north. Conditions like these are ideal to further investigate this field of work. These campaigns will also be collaborations with the Migration Ecology Group of the Department of Ecology.

The hope is that interesting results will be obtained and that LIF will provide new opportunities in the ecology research. Hopefully the technique could also spread and adapt to other areas as soon as the potential is discovered by others.

# Acknowledgements

This thesis work was sponsored by the Swedish Research Council and by a Linnaeus Grant to the Lund Laser Centre.

I would like to thank the other groups from Lund University with which we have cooperated throughout the work: the Aerosol Group of the Nuclear Physics Division who provided important reference data and the Migration Ecology Group and the Animal Ecology Group of the Department of Ecology for providing indispensable knowledge within biology.

All people at the Atomic Physics Division deserve appreciation for the general good will that has been shown in every aspect.

My supervisor Sune Svanberg has been a great support and I deeply value the time invested by him in educating me in all aspects of physics and research in general.

Especially I would like to thank my closest colleague and advisor Zuguang Guan, for instructing me in the handling of the lidar system and for great discussions.

I am grateful to the occasional and permanent members in the *Applied Molecular Spectroscopy and Remote Sensing Group* for showing good friendship.

Finally I thank Mikkel Brydegaard for teaching me a lot, including the fine art of handling cows.

# Appendix

## A.1. Ground references

As a reference value at ground level, data were provided by colleagues in the Aerosol Group of the Nuclear Physics Division at Lund University. These data are recorded with a nephelometer at the background station in Vavihill. In Fig. A.1-1, the extinction coefficient for particles at ground level is shown for three different wavelengths; 700, 520 and 450 nm. From these values an approximate extinction value at 355 nm is extracted. This value will be higher than any of the other since the scattering coefficient increases with decreasing wavelength.

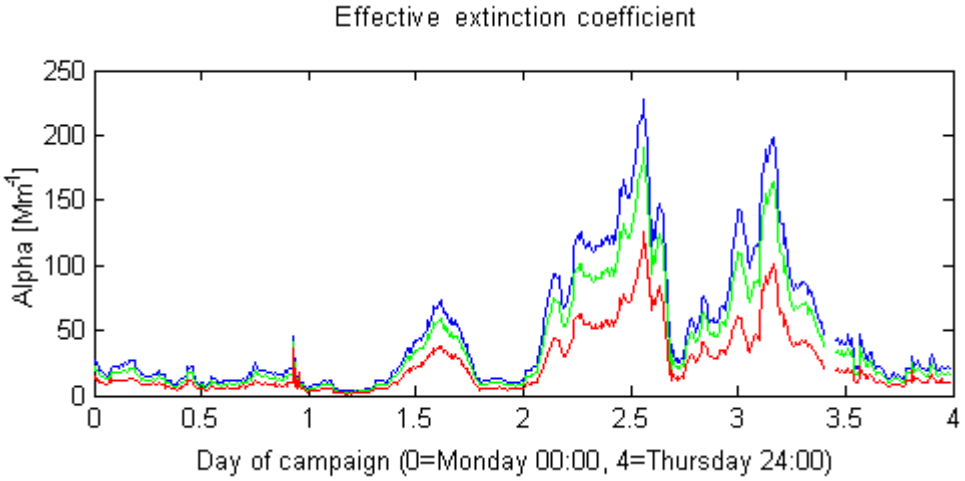


Fig. A.1-1. The effective extinction coefficient at ground level calculated with the help of a nephelometer. The curves represent the coefficients for 700 nm (bottom, red), 520 nm (middle, green) and 450 nm (top, blue). The value is referring to extinction from particles only. The x-axis is showing the time of the data recording. 0 is corresponding to Monday the 6$^{th}$ at 00:00 and 4 is Thursday the 9$^{th}$ at 24:00.

The extinction coefficient is the sum of the scattering- and absorption coefficients for particles. Provided by the Aerosol group are also calculations of the contributions from scattering and absorption, respectively. As expected, the absorption part is very low. In Fig. A.1-2, the absorption part only is shown for the days of the campaign.

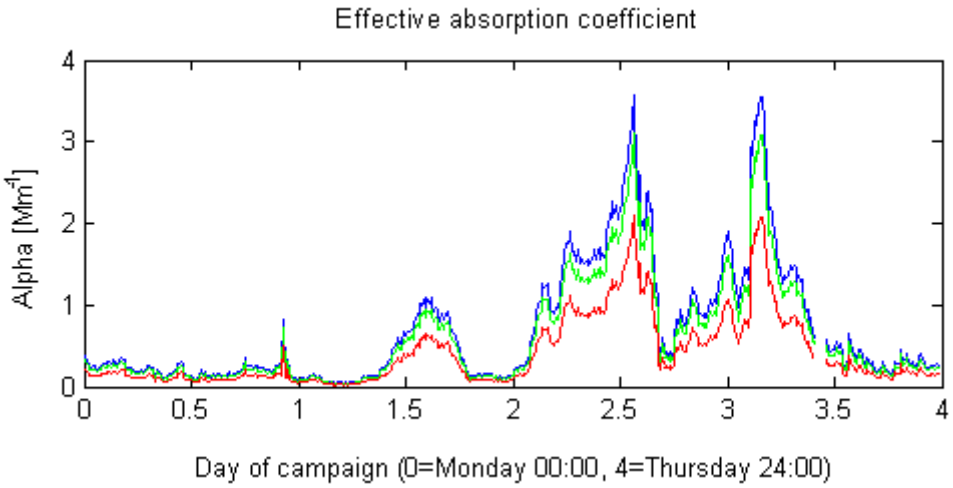


Fig. A.1-2. The effective absorption coefficient at ground level calculated with the help of a nephelometer. The curves represent the coefficients for 700 nm (bottom, red), 520 nm (middle, green) and 450 nm (top, blue). The value is referring to absorption only from particles.

As can be seen by comparing the numbers from the absorption and the extinction, the absorption is only around 1.5 % of the total extinction. The scattering is thus greatly dominant.

Also provided from the ground reference was the extinction-to-backscattering ratio, *S*. This is used in the Fernald inversion method. In Fig. A.1-3, the inverse of this ratio is shown for 700, 520 and 450 nm.

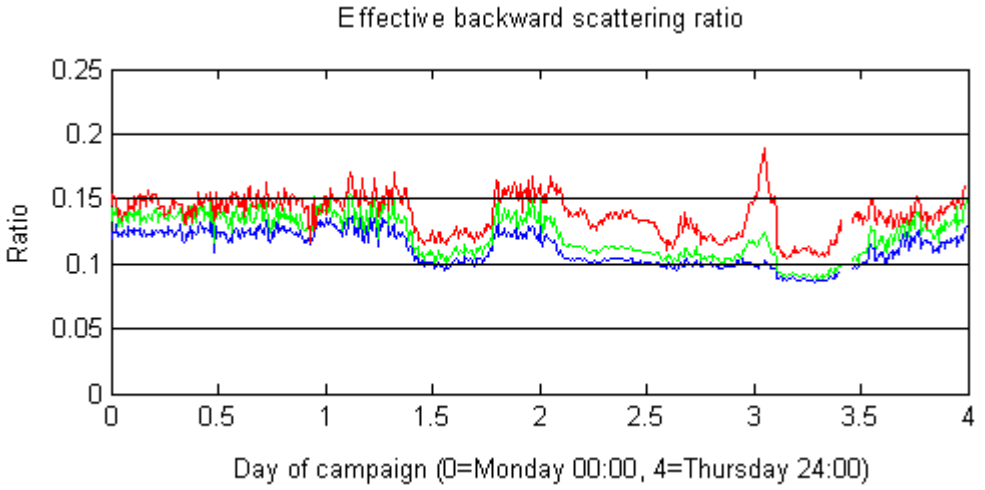


Fig. A.1-3. The backscattering ratio, shown for the wavelengths 700 nm (top, red), 520 nm (middle, green) and 450 nm (bottom, blue).

As can be seen in the figure, the ratio is decreasing with decreasing wavelength. To follow this trend, it is reasonable to believe that the ratio would be somewhat less for 355 nm than for 450 nm, reaching a mean value lying around 0.1 for the days of the campaign. In the calculations of the scattering coefficient, an S-value of 8.4 was used corresponding to an inverse value of 0.12.

## A.2. Photomultiplier tubes

Photomultiplier tubes, photomultipliers, or PMT's, are very fast and useful detectors for weak light. To be able to generate a readable signal from the weak light that arrives at the detecting position, some kind of amplification is needed, and PMT's are very effective for this purpose. The function of a PMT is best described by following what happens to a photon arriving at the detector.

The photon first hits the *photocathode*, positioned in the part of the PMT facing the "light source". The photocathode consists of a material that, through the photoelectric effect, releases electrons when struck by photons. The electrons released from the cathode are then accelerated by a high positive voltage toward the first of the *dynodes* in the dynode chain. The dynode, in its turn, then releases more electrons which are again accelerated by a voltage toward the second dynode, etc. In this way, more and more electrons are released for every dynode, resulting in a final number of electrons, arriving at the *anode*, being several orders of magnitude larger than the one released from the cathode. Typical is that this "avalanche effect" is amplifying the signal with up to a factor of one million [5].

In Fig. A.2-1, a schematic figure showing the most important parts of a PMT is presented.

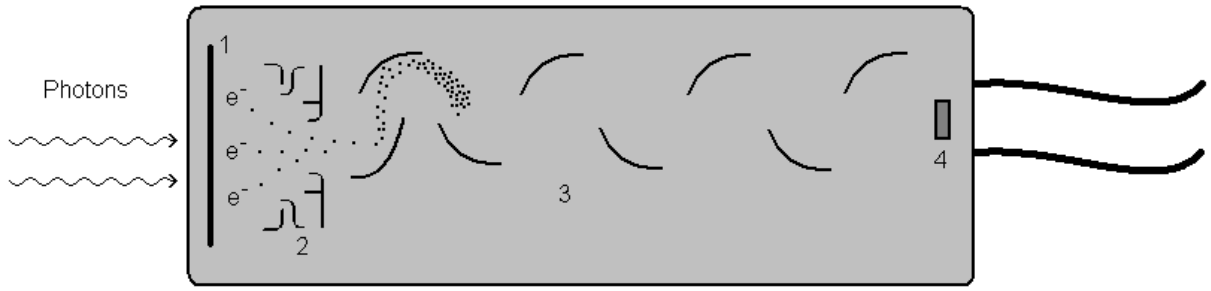


Fig. A.2-1. Schematic figure of the most important parts of a PMT: 1) Photocathode, 2) electron optics, 3) dynodes and 4) anode. A high voltage is applied between the cathode, anode and dynodes. The anode has a high negative potential which is then split over the dynodes to become zero at the cathode.

There are different materials to choose for the photocathode depending on the wavelength of light that should be detected. The material in the cathode has a specific *quantum efficiency* depending on wavelength, defined as the number of electrons (<1) released for every incoming photon. Today, however, many PMT's have a quite large wavelength span, in the visible- and the UV region.

## A.3. Impact of a second aperture in the detection system

We consider light that has been scattered at infinity ($a_1$) and at $R$ meters ($a_2$). The divergence of the beam is assumed to be zero (which of course is a considerable simplification). In Fig. A.3-1 a schematic figure of the geometry of the two apertures is shown. The telescope has again been represented by a lens.

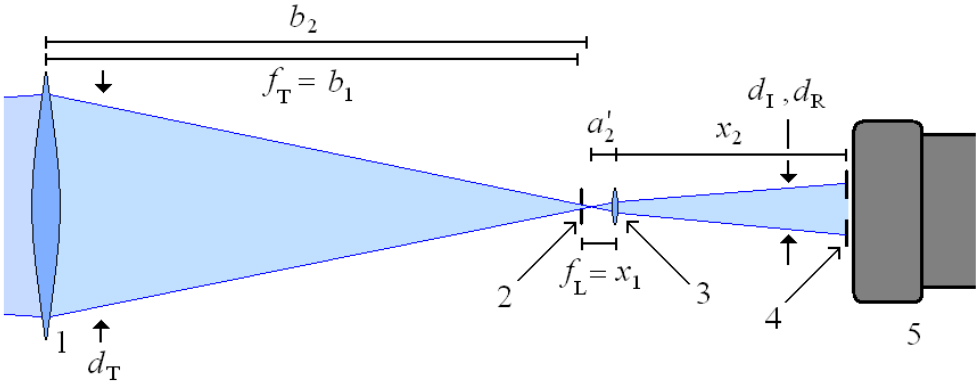


Fig. A.3-1. Schematic layout of the optics considered. In the figure are included the telescope (1), the first aperture (2), the collimating lens (3), the second aperture and the PMT (5). The figure is not to scale.

The focal length, $f_T$, of the telescope is 1 m [25]. According to geometrical optics, the distance, $b$, from the telescope to the focus of the light is given by Eq. A.3-1.

$$\frac{1}{b} = \frac{1}{f} - \frac{1}{a} \,, \tag{A.3-1}$$

where $f$ is the focal length and $a$ is the distance between the scattering event and the telescope.

The distances from the telescope to the focuses are then $b_1$ = 1.0000 m and $b_2$ = 1/(1/1-1/$R$). The collimating lens is positioned approximately $x_1$ = 1 cm behind the first aperture. To calculate the behavior of the light after this lens this, we again use A.3-1. The lens is assumed to be perfectly collimating for the light scattered at infinity and thus its focal length, $f_L$, should be: $f_L$= 1 cm.

The spot diameters, at the position of the second aperture, $x_2$ = 10.5 cm behind the lens, for the light scattered at infinity ($d_I$) and $R$ m ($d_R$) becomes:

$$d_1 = \frac{f_L}{f_T} \cdot d_T = 4\text{mm} \,, \tag{A.3-2}$$

$$d_R = \frac{a_2'}{b_2} \cdot d_T \left( 1 + \frac{x_2}{-b_2'} \right), \tag{A.3-3}$$

where $d_T$=40 cm is the size of the telescope [25], $a_2$'=$f_L$-($b_2$-$f_T$) and $b_2$'= 1/(1/$f_L$-1/$a_2$').

The two sizes of the apertures in the second position are 8 and 20 mm. The spot size of the light scattered at infinity is clearly always small enough to pass through both aperture sizes. This is, however, not the case for the light scattered at the distance *R*. Fig. A.3-1 shows a simulation of the ratio between the amount of light that passes through the small aperture and that which passes through the large as a function of distance, *R*.

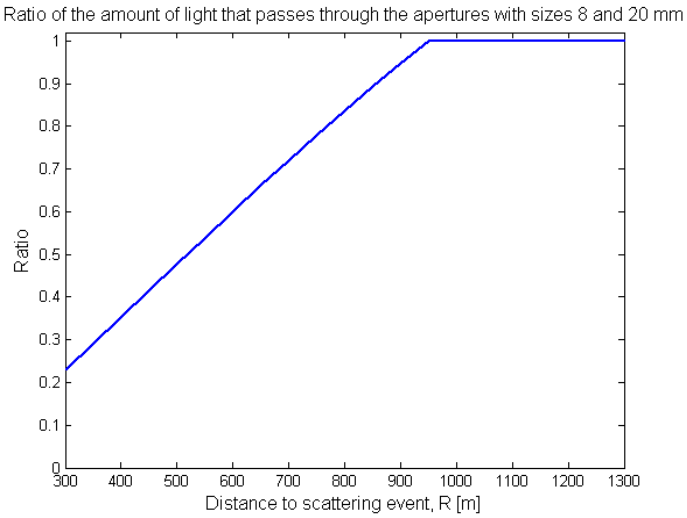


Fig. A.3-1. Simulation of the effect of apertures after the focal plane of the telescope.

As can be seen, the appearance of this figure is similar to Fig. 1.4-7. The exact numbers are however not the same. That is because the calculations here are very primitive and only the most important effects are considered. The purpose is only to prove that the behavior is reasonable, which might not be clear when the aperture is not in the focal plane. The experimental curve is of course the true one where all physical effects that are not considered here are included.

# A.4. Pictures of discussed bird species studied

Fig. A.4-1. Birds used in the measurements with 355 nm illumination. On top from the left: Robin (*Erithacus r. rubecula*), Blue tit (*Parus careuleus*) and Jackdaw (*Corvus monedula*). On the bottom from the left: European reed warbler (*Acrocephalus s. scirpaceus*) and Starling (*Sturnus v. vulgaris*).

.

Fig. A.4-2. Birds used in the measurements with 266 nm illumination. Top from the left: Rook (*Corvus f. frugilegus*) and Great reed warbler (*Acrocephalus arundinaceus*). Bottom from the left: Starling (*Sturnus v. vulgaris*) and Black cap (*Sylvia atricapilla*).

## A.5. LIF measurements on damselflies

The LIF measurements on birds were as stated performed in close connection to lidar studies on damselflies. The experiments on the two different animal types are closely related and similar approaches were used. In this section the experiments on the insects are very briefly introduced as a complement to the measurements on birds presented in Chap. 2. A background to the studies can be found in [38] and a detailed description of the field work is found in [37].

Analogous to birds, the beautiful insects damselflies, being ectotherms, are forced to change their habitats according to global temperature changes. It has turned out that these animals consistently have moved their living locations northwards during the last years [39]. The damselflies are therefore possible effective natural probes for climate changes. With remote investigations, the risk of disturbing the natural behavior of the animals is also decreased.

The site at Klingavälsån is a position where much research has been done on these insects, by among others scientists from the Animal Ecology group in Lund. The purpose of the corresponding measurements was to try to observe several different features of the damselflies, e.g., where they are mostly located at and around the river and how they are affected by weather and time of day, i.e., when they start to fly in the morning and when they stop in the evening (they are generally not flying at night). One aim was also to try to discriminate between different species and genders, similar to the studies on birds.

The two species of damselflies that were mainly studied in this field work were *Calopteryx splendens* and *Calopteryx virgo*, both shown in Fig. A.5-1.

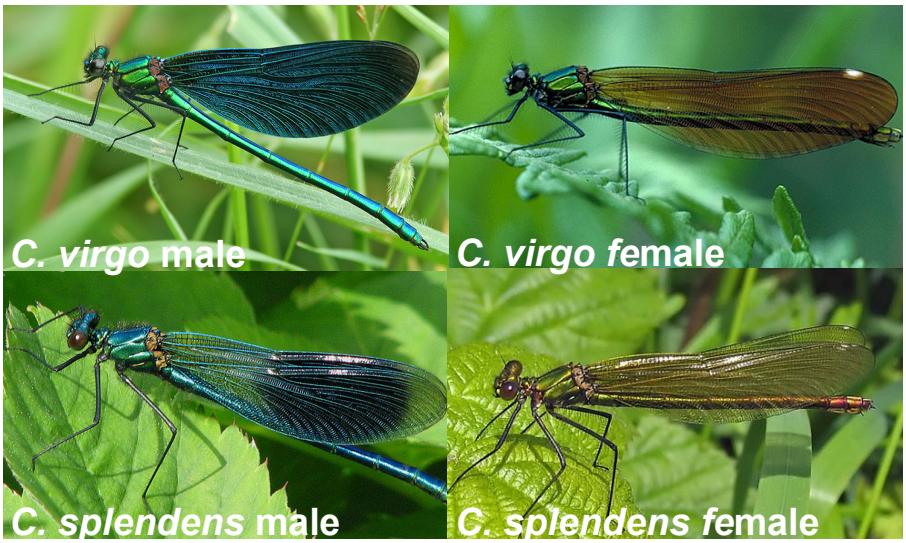


Fig. A.5-1. Photographs of females and males of the two examined species of damselflies.

During the experiments, the laser light was sent out in three different directions over the river. Positions were chosen with the possibility to reach close to the surface of the water, which is where the insects appear to spend most time. The beam should also stay close over the river for as long distance as possible to increase the chance of detecting insects. Fig. A.5-2 shows a view of the experiment field from above.

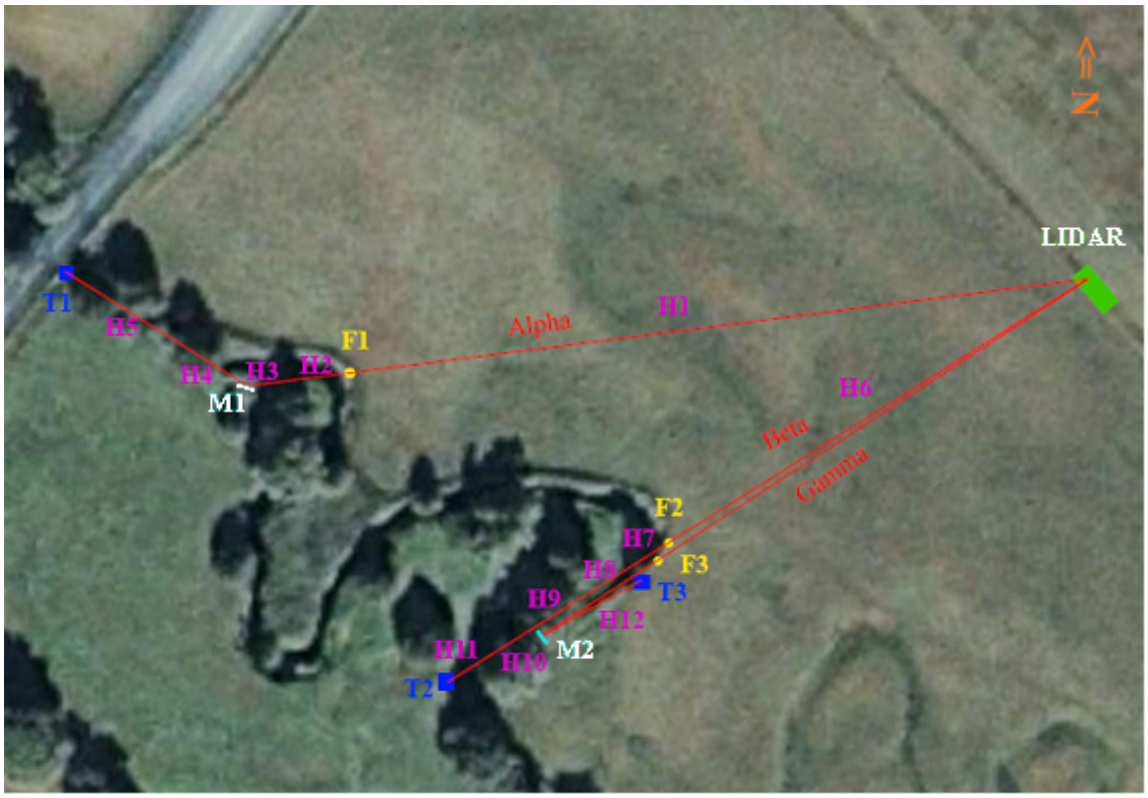


Fig. A.5-2. Overview of the geometry for the experiments on damselflies at the river Klingavälsån.

Included in the figure are the position of the lidar equipment on the dirt road, the three beam directions, *Alpha*, *Beta* and *Gamma*, the three terminations points, *T1*, *T2* and *T3*, the positions where the beam passed through a metal fence, *F1*, *F2* and *F3* and two positions of a folding mirror, *M1* and *M2*. The folding mirror was used to redirect the beam to be able to keep a longer light path close to the water surface.

The exact same geometry applies to the bird measurements, and the approximate positions of both the flying birds and the museum samples are in the figure close to *F2*.

The echo signals from the damselflies were collected in the three colour bands used to observe the birds, namely, elastic light, fluorescence between 400 and 500 nm and between 500 and 750 nm. The strength of the signals in the three channels can then be used to discriminate between the blue and green insects in a similar manner to the bird measurements.

# References

[1] K. Noone: *The indirect radiative effect of aerosols*, IGAC Newsletter – Issue 23 – Atmospheric chemistry, aerosols and climate, (2001).

[2] J. Shaw, N. Seldomridge, D. Dunkle, P. Nugent, L. Spangler, J. Bromenshhenk, C. Henderson, J. Churnside and J. Wilson: *Polarization lidar measurements of honey bees in flight for locating land mines*, Opt. Expr., Vol. 13, p. 5853, (2005).

[3] M. Brydegaard, P. Lundin, A. Runemark, Z. Guan, S. Åkesson and S. Svanberg: *Feasibility study: fluorescence lidar for remote bird classification*, to appear.

[4] S. Slanina: *Environmental problems caused by local air pollution*, The Encyclopedia of Earth, (2008).

[5] S. Svanberg: *Atomic and molecular spectroscopy, 2nd edition*, Springer-Verlag, p. 115, (1992).

[6] G. Ohring: *The effect of aerosols on the temperatures of a zonal average climate model*, Pageoph, Vol. 117, p. 851, (1979).

[7] M. O. Andreae, C. D. Jones and P. M. Cox: *Strong present-day aerosol cooling implies a hot future*, Nature, Vol. 435, p. 1187, (2005).

[8] T. L. Anderson, R. J. Charlson, S. E. Schwartz, R. Knutti, O. Boucher, H. Rodhe and J. Heintzenberg: *Climate forcing by aerosols – a hazy picture*, Science, Vol. 300, p. 1103, (2003).

[9] *Atmospheric aerosols: what are they, and why are they so important?*, NasaFacts Online, (2006).

[10] J. Quaas: *Smoke and climate change*, Science, Vol. 325, p. 153, (2009).

[11] G. Myhre: *Consistency between satellite-derived and modeled estimates of the direct aerosol effect*, Science, Vol. 325, p. 187, (2009).

[12] M. Andersson and P. Weibring: *A user friendly lidar system based on LabVIEW*, Lund Reports on Atomic Physics, LRAP-201, (1996).

[13] N. Takeuchi: *Elastic lidar measurements of the troposphere*, in T. Fujii and T. Fukuchi: *Laser remote sensing*, Taylor & Francis Group, p. 67, (2005).

[14] R. Penndolf: *Tables of the refractive index for standard air and the Rayleigh scattering coefficient for the spectral region between 0.2 and 20.0 μ and their application to atmospheric optics*, JOSA, Vol. 47, p. 176-182, (1957).

[15] E. Boeker and R. von Grondelle: *Environmental science: physical principles and applications*, John Wiley & Sons Ltd., (2001).

[16] J. Harms, W. Lahmann and C. Weitkamp: *Geometrical compression of lidar return signals*, Appl. Opt., Vol. 17, p. 1131, (1978).

[17] P. A. Davis: *The analysis of lidar signatures of cirrus clouds*, Appl. Opt., Vol. 8, p. 2099 (1969).

[18] J. D. Klett: *Stable analytical inversion solution for processing lidar returns*, Appl. Opt., Vol. 20, p. 211, (1981).

[19] F. G. Fernald: *Analysis of atmospheric lidar observations: some comments*, Appl. Opt., Vol. 23, p. 652, (1984).

[20] H. Kinjo, H. Kuze, T. Takamura and N. Takeuchi: *Derivation of aerosol extinction-to-backscattering ratio using a multi-wavelength lidar and a sun photometer*, International Laser Sensing Symposium, 20th Japanese Laser Sensing Symposium (ILSS'99) Abstracts of Papers, Sept. 6-8, Fukui, p. 41, (1999).

[21] Y. Sasano and E. V. Browell: *Light scattering characteristics of various aerosol types derived from multiple wavelength lidar observations*, Appl. Opt., Vol. 28, p. 1670, (1989).

[22] G. Andersen, J. K. Brasseur, R. J. Knize and P. Haris: *Raman and Rayleigh holographic lidar*, Appl. Opt., Vol. 41, p 1798, (2002).

[23] Y. M. Noh, Y. J. Kim, B. C. Choi and T. Murayama: *Aerosol lidar ratio characteristics measured by a multi-wavelength Raman lidar system at Anmyeon Island, Korea*, Atmospheric Research, Vol. 86, p. 76, (2007).

[24] V. A. Kovalev: *Determination of slope in lidar data using a duplicate of the inverted function*, Appl. Opt., Vol. 45, p. 8781, (2006).

[25] P. Weibring, H. Edner and S. Svanberg: *Versatile mobile lidar system for environmental monitoring*, Appl. Opt., Vol. 42, p. 3583 (2003).

[26] D. M. Powell, J. A. Reagan, M. A. Rubio, W. H. Erxleben and J. D. Spinhirne: *Micropulse lidar Tenerife, Canary Island observations*, Proceedings of the Eighth Annual ARM Science Team Meeting, p. 619, (2008).

[27] M. Devi, A. K. Barbara, M. Saikia and W. Chen: *Vertical distribution of optical parameters of aerosols using portable automatic lidar system of Gauhati University*, Indian Journal of Radio & Space Physics, Vol. 37, p. 333, (2008).

[28] J. A. Reagan: *New generation lidars to support aerosol radiation/climate forcing studies*, Symposium Proc. IGARS'95, Florence, Italy, p. 2313, (1995).

[29] M. R. Paulson: *Lidar measurements indicating atmospheric inhomogeneities*, Final Report, 1 Jul. - 31 Oct. 1985 Naval Ocean Systems Center, San Diego, CA, (1986).

[30] V. A Kovalev: *Stable near-end solution of the lidar equation for clear atmospheres*, Appl. Opt., Vol. 42, p. 585, (2003).

[31] A. Weber: *Raman spectroscopy of gases and liquids*, Spriger-Verlag, Vol. 11, p. 318, (1979).

[32] J-Y. Ku, C. Hogrefe, G. Sistla, S. Chaw, L. Charles and B. Gross: *Use of lidar backscatter to determine the PBL heights in New York city, NY*, Models-3 Users' Workshop, Chapel Hill, NC, (2006).

[33] P. Chazette, J. Sanak and F. Dulac: *New approach for aerosol profiling with a lidar onboard and ultralight aircraft: application to the African monsoon multidisciplinary analysis*, Environmental Science & Technology, p. 8335, (2007).

[34] R. L. Rowell and G. M. Aval: *Rayleigh-Raman depolarization of laser light scattered by gases*, J. Chem. Phys., Vol. 54, p. 1960, (1971).

[35] A. C. Eckbreth: *Laser diagnostics for combustion temperature and species, 2nd edition*, Gordon and Breach Publishers, p. 15, (1996).

[36] G. E. Hill and K. J. McGraw: *Bird coloration: function and evolution*, Harvard University Press, p. 357, (2006).

[37] Z. Guan, P. Lundin, M. Brydegaard, M. Wellenreuter and S. Svanberg: *Insect monitoring with fluorescence lidar techniques: field study*, to appear.

[38] M. Brydegaard, Z. Guan, M. Wellenreuter and S. Svanberg: *Insect monitoring with fluorescence lidar techniques: feasibility study*, Appl. Opt., Vol. 48, p. 5668, (2009).

[39] C. Parmesan: *Ecological and evolutionary responses to recent climate change*, Annu. Rev. Ecol. Evol. Syst. 37, p. 637, (2006).